NuSTAR Calibration Plan

Date: September 16, 2010

Authors: W. Craig, B. Grefenstette, F. Harrison, C. Hailey, J. Koglin
Maintained by: F. Harrison

Approved by:

_____
Fiona Harrison, PI

_____
Bill Craig, Instrument Manager

_____
Charles Hailey, Optics lead

_____
Finn Christensen, Optics calibration scientist

Release Notes:

Versions prior to 3.0 were working versions and not configuration controlled.

Version 3.0 Draft version sent to calibration review board

Version 3.1 Responds to comments from calibration board. Still needs development of in-flight calibration plan, in particular addition of simulations with updated response matrices, and discussion of schedule for regular routine calibration.

1. Overview

This document describes the calibration plan for the NuSTAR instrument. The main document describes the requirements, overall approach, in-flight calibration, and summarizes the plans for the optics modules, focal plane detectors, and detector entrance windows and optics thermal cover. Appendices are included that provide details of the experimental setup, error budgets, and specifics of the measurements for both optics and focal plane detectors.

2. Calibration Requirements

2.1 Science Calibration Requirements

The level 2 calibration requirements describe the final calibration accuracies that must be achieved in-flight from a combination of ground and in-flight calibration in order to meet the scientific objectives. This includes any changes that occur due to the orbit environment, aspect knowledge uncertainties, and gradual changes over the two-year baseline mission. The requirements, listed below, are maintained under configuration control in the NuSTAR Science Requirements Document (JPL D-41835). In case of any discrepancy, the requirements document is the master version.

2.1.1 Absolute Flux Calibration

The systematic contribution to flux measurement uncertainties (δf/f) in the 6-10 keV band, for a point source with a power law photon spectral index of 1.7, shall be less than 15% (3-sigma) over the central 2x2 arcminutes of the FOV.
Context : This is required in order to tie flux measurements to other soft X-ray observations and applies to point sources (derives from blazar objective). The systematic contribution refers to error in flux determination for a measurement where statistical errors are negligible.
ID : L2-SCI-146

The systematic contribution to flux measurement uncertainties (δf/f) in the 6-10 keV band, for a point source with a power law photon spectral index of 1.7, shall be less than 30% (3-sigma) over the central 11x11 arcminutes of the FOV.
Context : This requirement is driven by galactic and extragalactic survey objectives and applies over the entire FOV excluding the edges. In particular, it is driven by the desire for hardness ratio measurements to be dominated by statistical rather than systematic errors.
ID : L2-SCI-147

The systematic contribution to flux measurement uncertainties (δf/f) in the 10-30 keV and 30-79 keV bands, independently and for a point source with a power law photon spectral index of 1.7, shall be less than 30% (3-sigma) over the central 11x11 arcminutes of the FOV.

Context : This requirement is driven by galactic and extragalactic survey objectives and applies over the entire FOV excluding the edges. In particular, it is driven by the desire for hardness ratio measurements to be dominated by statistical rather than systematic errors.
ID : L2-SCI-148

The systematic contribution to absolute flux measurement uncertainties (δf/f) for monochromatic line sources in the 60-79 keV band shall be less than 15% (3-sigma) over the central 8x8 arcminutes of the FOV.
Context : This is driven by the desire to have measurements of the ^{44}Ti yield in supernova remnants limited by uncertainties in the distance to the objects.
ID : L2-SCI-149

2.1.2 Spectral Calibration

The systematic contribution to measurement of a power law spectral index α (for a source characterized by $F=kE^{-\alpha}$ with $-1<\alpha<1$ and F in units of erg/cm^2/s/keV) shall be less than 0.15 (3-sigma) in the 6-10 keV, 10-30 keV, and 30-79 keV bands, independently and for any point in the central 11x11 arcminutes of the FOV.
Context : This is driven by the galactic survey objective to classify sources by constraining spectral shape.
ID : L2-SCI-151

The systematic contribution between 60 and 79 keV to measurement of a power law spectral index α (for a source characterized by $F=kE^{-\alpha}$ with $-1<\alpha<1$ and F in unites of erg/cm^2/s/keV) shall be less than 0.15 (3-sigma) for any point in the central 8x8 arcminutes of the FOV.
Context : This is driven by the 44Ti supernova remnant objective. It will be important to pin the underlying continuum to fit line shapes, and we need some bandpass over which to do this; hence, the 60 keV lower limit.
ID : L2-SCI-153

2.1.3 Point Spread Function Characterization

The integrated value of the instrument point spread function from 70%-90% encircled energy shall be determined to 10% (3-sigma) over the central 11x11 arcminutes of the FOV.
Context : This is driven by the galactic survey mapping of diffuse features in the vicinity of point sources.
ID : L2-SCI-155

The instrument point spread function shall be determined as a function of radius to 3% (3-sigma) at all radii out to 70% encircled energy over the central 11x11 arcminutes of the FOV.
Context : This is driven by the requirement to accurately remove point sources embedded in diffuse features in the Galactic Center region.
ID : L2-SCI-159

The instrument point spread function shall be determined as a function of azimuth to 10% (3-sigma) at all azimuthal angles and at all radii out to 70% encircled energy over the central 11x11 arcminutes of the FOV.
ID : L2-SCI-160

2.2 Instrument Level 3 Calibration Requirements

The instrument Level 3 calibration requirements are derived from the L2 science calibration requirements. They represent the instrument parameters that must be determined through a

Alignment	**Requirement**	**Rationale**
Optical Axis Knowledge	15"	Throughput determination
Effective Area		
Absolute effective Area: 6 -10 keV - central 2' x 2'	15%	Cross calibration with low-energy missions
Absolute effective area: 6 - 10, 10 - 30, 30 - 79 keV bands - 11' x 11'	25%	Hardness ratio determination, surveys
Absolute effective area in each 2 keV bin between 60 - 80 keV	12%	^{44}Ti yield measurement
Relative effective area in each 2 keV bin between 6 and 79 keV over central 8' x 8'	5%	Spectral index fitting, bright sources
Relative effective area in each 2 keV bin 60 - 79 keV in central 8' x 8'	3%	Continuum modeling and subtraction ^{44}Ti
Point Spread Function		
Integrated PSF 70-90% encircled energy over 11'x11'	10%	Mapping diffuse features/point sources
PSF as function of radius out to 70% encircled energy	3%	Flux determination. Remove point sources in diffuse emission
PSF as function of azimuth out to 70% encircled energy over 11' x 11'	10%	Mapping diffuse extended features, jets

combination of ground and on-orbit calibration in order to meet NuSTAR's scientific objectives. Note that these requirements refer to the knowledge of the given parameter on-orbit, including all sources of uncertainty. They are listed in Table 1.

3. Calibration Approach

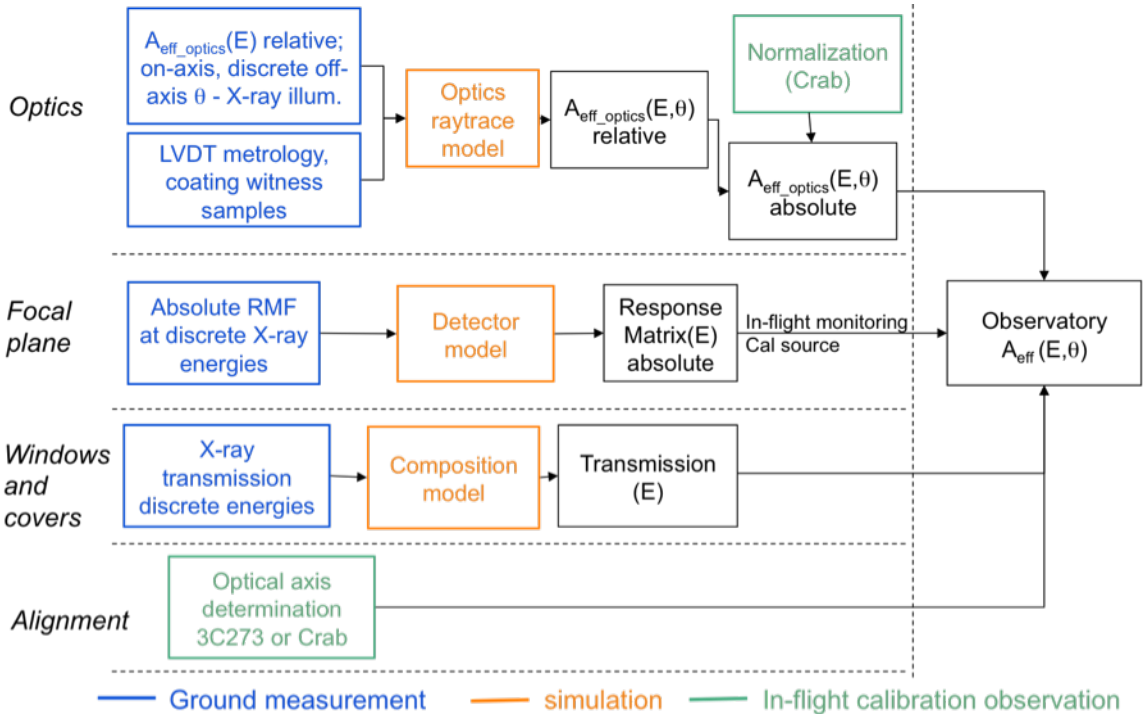

The calibration of the instrument effective area relies on a combination of ground and in-flight measurements. Figure 1 shows a schematic of the calibration strategy. The relative optics effective area will be measured on-axis and at discrete off-axis angles as a function of energy using an X-ray beam. These measurements will be combined with measurements of the reflectance of flight coatings obtained from witness samples, and mechanical metrology of the optic to build a raytrace model that will be used to generate the relative effective area for all angles and energies. The focal plane will be calibrated to get the absolute response at discrete energies, and this combined with data from spatial mapping of the response will be used to generate a response model for the detectors. The transparency of the optics thermal cover and detector entrance window will be measured at discrete energies and a model of the composition used to obtain the throughput as a function of energy. In order to obtain the overall instrument effective area two things must be determined using in-flight calibration: 1) the absolute normalization of the optics area curve, and 2) the location of the optical axes on the focal planes. The first item will be determined using measurements of the Crab, which can be cross referenced to observations in the 6 – 10 keV band from XMM, Chandra and other soft X-ray telescopes to find the optics area normalization. The location of the optical axis will be determined from observations of the Crab pulsar and/or 3C273.

The instrument point spread function will be calibrated on-orbit using the bright point source Cygnus X-1.

4. Ground Calibrations

This section describes the ground measurements that will be made in order to build accurate models that will ultimately be used to generate calibration files. As described above, in-flight measurements are required to determine the overall normalization of the optics response as well as determine the PSF to the requisite accuracy for science analysis. It is important to note that for both optics and detectors we are not directly measuring the response, but rather making measurements at discrete energies and incidence angles that will be used to build raytrace (in the case of optics) and Monte Carlo/charge transport models (in the case of the focal plane). The models must be used to properly interpolate in energy and angle. Further, it should noted that there will be no end-to-end calibration of the X-ray telescope after the elements are integrated into the instrument. Although not formally part of the calibration plan, the NuSTAR verification and validation activities do include the broadband hard X-ray illumination of an EM focal plane module by FM0 at the Nevis calibration facility to provide validation of the system performance model.

The subsections below describe the ground calibrations that will be made for optics, focal plane, windows and thermal covers.

4.1 Optics

4.1.1 Calibration requirements

The optics ground calibration requires only determination of the relative effective area as a function of energy and off-axis angle (although an absolute area determination will be made for verification purposes using the measurements). In order to meet the instrument L3 requirements, the following optics calibration requirements are derived:

The relative effective area of each optics module, for x-ray energies between 6 and 60 keV and over the central 8' by 8' of the field of view, shall be determined to at least 3% in each 2 keV bin.
ID : L4-OPTICS-150

The relative effective area of each optics module, for x-ray energies between 60 keV and 79 keV over the central 8' by 8' of the field of view, shall be determined to at least 2% in each 1 keV bin.
ID : L4-OPTICS-151

4.1.2 Optics calibration approach

The primary goal of the ground flight optics calibration is to use X-ray measurements of the effective area both on and off-axis as a means to verify the optics response model (ORM). This requires an extremely good measurement of the relative effective area as a function of energy. There are several secondary goals including measurement of the flight optics point spread response

function (PSF) and a measurement of the absolute effective area of the flight optics at select energies. These secondary goals are necessary to verify that the optics subsystem meets its level 4 performance requirements, and they will be useful as a cross-check on the overall science calibration. However, we do not formally place calibration requirements on the absolute measurements because the challenging nature would drive cost and schedule, and because we believe that combined with on-orbit measurements and absolute knowledge of the focal plane response we will meet the overall science requirements.

A very general description of the calibration approach and philosophy is provided here. A brief discussion of how the particulars of this approach help control systematic errors relevant to the effective area determination is also provided. The actual detailed calibration procedure is presented later in the document, in Appendix B.

The ground calibration requirements relate only to determination of the relative effective area as a function of energy and off-axis angle. We note that the PSF will be characterized in order to verify that it meets requirements, but, like the absolute response, this is not considered necessary from a calibration perspective.

Overview of Calibration Facility

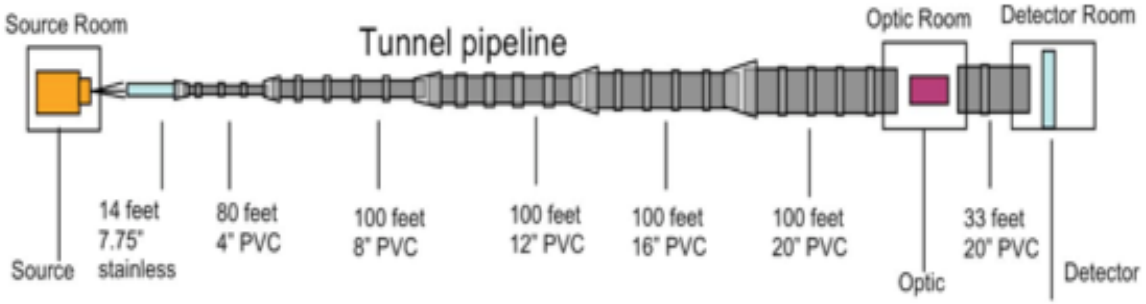

Figure 1 Overview of the RaMCaF beamline.

The X-ray calibration facility is located at Columbia University's Nevis Laboratory in Irvington, NY. The facility, officially the Rainwater Memorial Calibration Facility (RaMCaF) is housed in an existing 160m long tunnel previously used for high-energy physics experiments. At the source end of the tunnel, a Comet MXR-160 x-ray tube with tungsten target provides a broad band bremsstrahlung ~7.5mm diameter source with a spectrum and intensity as shown below. The beam exits the tube through a 4-position filter holder, a beam shaper (attenuator) and a 15mm diameter collimator before entering an evacuated pipe. The length from the tube exit to the pipe is at ambient air pressure. The beamline is constructed primarily of PVC pipe and is pumped down to ~1 torr. The beam exits the 160m tube through a Mylar/Kevlar window into a cleanroom which houses the optic module.

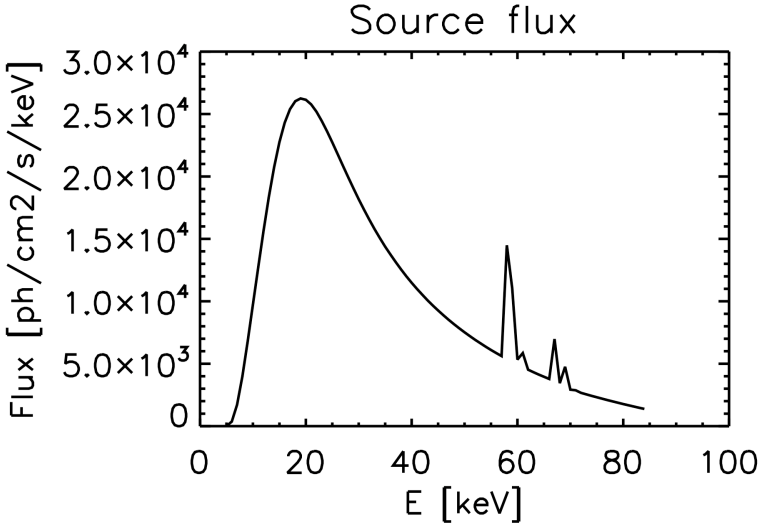

Figure 2 Spectrum (ideal) of X-ray beam

The optics module is mounted in a motorized fixture that allows control of 5 degrees of freedom (2 translation, 3 rotation). The beam exits the optic cleanroom and enters through a second Kapton/Mylar window, through another 10 m PVC pipe, also pumped to ~1 torr vacuum, and exits through a similar window into a separate room which houses the detector and slits. The primary detector is a non-imaging Ge coax which can be translated over 200mm. Two crossed one-dimensional slits sit in front of the detector and are mounted on an independent translation stage that allows the slit assembly to be moved with respect to the detector. A SiLi detector is used for low energy measurements and an imaging detector, based on a scintillator coupled to a CCD, can take the place of the Ge detector for appropriate measurements.

A Labview-based data taking and control system controls and monitors the configuration of the source, stages, housekeeping and detectors. All data is logged in FITS format to a web server accessible to all members of the NuSTAR team.

Effective Area Measurements

The effective area measurement will be performed 3 ways. The first is through a full flood illumination of the optic. The second is through a full flood illumination of an entire figure of revolution, but restricting the radial extent of illumination to a multilayer group (actually subgroup, see below). The third is through measurements restricted in both azimuthal and radial extent. Together these 3 sets of measurements can be employed to both determine effective area and perform self-consistency checks on the analysis. The third approach provides the best data set for constraining the optics response function.

The measurement of $I_o(E)$ (the through X-ray beam measurement without optic) and I(E) (the X-ray beam after reflection off of the optic) are done using a Germanium spectrometer. Normally, if a an X-ray source or radioactive source is available with lines sufficiently narrow that the effective area A(E) is constant over the linewidth, a simple ratio (with at most a small correction) of I/I_o yields the energy dependent effective area. However the use of a continuum X-ray source for the

NuSTAR calibrations requires a more involved procedure. The approach is to parametrically model the X-ray source spectrum based on the through beam data, and then fold this derived X-ray source spectrum with an effective area curve (suitably parameterized for multilayer reflectivity, roughness, contamination etc.), detector response function and various transmission and geometric factors to fit the observed reflected X-ray beam and thus determine the effective area. In this procedure, the detector model is fixed based on extensive calibrations with known radioactive sources that have been used to derive a GEANT model of the detector system, including scattering in the housing. It should be noted that this Ge detector has been cross-calibrated against an RHESSI flight spare unit at Caltech. The optics effective area as a function of energy for the illuminated region will be derived by adjusting model parameters until the model matches the measurements. By limiting the illuminated area to a multilayer subgroup and restricted input angular range we minimize the number of parameters that need to be adjusted to fit each measurement. That is why we consider the limited aperture measurements to be the cleanest data with which to calibrate the optics response mode.

This approach requires careful attention to systematic effects, even if only a relative effective area curve is desired. While the primary goal is to obtain good relative effective area over the NuSTAR energy band (since absolute effective area will be obtained from in-flight calibration), the above approach directly yields absolute effective area (with larger uncertainties). Thus the optics calibration will provide a cross-check on in-flight absolute area calibration, along with a much better relative effective area calibration. As mentioned below, for the energy region below ~15 keV, a Silicon detector, with excellent energy resolution, will augment the baseline Ge spectrometer measurements. A Si beam monitor will be in place continuously to record absolute intensity and spectral shape of the beam; this is particularly important at energies below 10 keV.

Detailed measurements of through and reflected X-ray beams for each multilayer group will be done over a range of incidence angles from on-axis to well off-axis, and also over the entire NuSTAR energy band. The data acquisition will be done by restricting the X-ray beam to less than a single multilayer group (the 10 multilayer groups will be divided into 20 subgroups) and to a limited azimuthal sector through the use of aperture plates. At a minimum, 40% of the optic effective area will be probed in this fashion and up to 100%, time permitting. Using a restricted azimuthal sector and a radial extent limited to the multilayer subgroups provides the most constraining data set for validating the optics response model. In addition, it permits tailored masking of the focal plane to suppress single reflection X-rays. The X-ray through beam is characterized both before and after X-ray reflectivity measurements. This permits monitoring of X-ray source temporal and spectral stability, along with any variations in count rate caused by change in scattering and absorption in the beam due to pressure, temperature and humidity variations in residual beam pipe gas and the air path in the optics and detector rooms. The through beam is characterized by moving the optic out of the X-ray beam, ensuring a constant viewing factor for the X-ray source. These measurements provide adequate statistical sampling to reconstruct the effective area as a function of angle and energy and to validate the optics response model. This data is then used to interpret data from full figure of revolution illumination of the optic.

In addition to these reflectivity measurements restricted in both azimuthal and radial sector, reflectivity will be measured for the full figure of revolution. This will be done by using aperture plates which mask off each of the 20 multilayer subgroups, but permit full 360 degree azimuthal

illumination. These measurements will also be done over the full range of incidence angle and the entire energy band.

Imaging Measurements

The encircled energy function (EEF) will be measured 2 ways. Imaging measurements are performed as a natural outcome of the alignment procedure. The alignment is done with a full figure of revolution aperture plate, restricted to a multilayer subgroup. Once the X-ray axis of the optic is determined by scanning in pitch and yaw, the encircled energy function can be directly determined by interrogating the image spot using a scanning slit positioned in front of the focal plane. The EEF will be determined at a range of incidence angles and all energies for each multilayer subgroup. The second EEF measurement will be done with a simple on-axis full-flood illumination. This will provide a cross-check data for the on-axis subgroup images.

Control of Systematic Effects

The ground calibration of the flight optics is particularly challenging because of the broad energy band covered by NuSTAR (6-78 keV). The difficulties are exacerbated by the need to have a very good relative effective area calibration in the 6-10 keV region, where the energy overlap with major X-ray observatories with focusing optics (e.g. Newton, Chandra, Astro-E) exists. The NuSTAR flight optics calibration is complicated at these low energies because of 1) emission line structure from the X-ray source 2) the complicated response of the calibration detectors in this energy band due to the presence of X-ray escape peaks and scattering of higher energy source X-rays and 3) structure in this energy band due to multilayer coatings and 4) significant absorption in beamline gas and transmission windows (complicating response function modeling). An additional complication is that the multilayer coatings are divided into 10 separate coating formulations, and these provide substantially different effective area responses as a function of energy and graze angle.

In order to control for systematic effects in the effective area determination it is crucial to do the following; control and monitor X-ray source spectral and temporal stability; obtain the most accurate low energy detector response matrix; minimize, to the extent possible, low energy cutoffs due to windows and gas in the beamline; isolate multilayer recipe groups for separate calibration. Below is a brief description of how the chosen calibration approach permits control of systematic effects important in modeling.

It is crucial to control the X-ray source parameters during calibration. At soft X-ray energies it is quite common to use X-ray fluorescence or radioactive line sources to provide an $I_o(E)$ (X-ray through beam intensity as a function of energy) which is effectively has a delta function response with energy (ie., the change in the effective area A(E) is negligible over the energy line width of the through beam). Thus the spectral dependence of the X-ray source intensity effectively drops out of the calculation of optics effective area. However the use of a continuum X-ray source on NuSTAR optics calibrations means that the X-ray source spectrum must be well-characterized, and thus spectral and temporal stability are very important, since there is substantial redistribution of energy in the detector.

This is addressed by 1) obtaining I(E) and $I_o(E)$ measurements by moving the optic in and out of the X-ray beam, while the X-ray source always transits the same aperture 2) taking optics measurements over timescales short enough so that the X-ray source is known to be spectrally and temporally stable 3) frequent measurement of the X-ray source intensity $I_o(E)$ and 4) continuous monitoring of the flux at the detector focal plane using a Si diode with good low energy response.

The frequent measurements of X-ray source intensity are also important for controlling environmental systematics. The residual gas in the beamline and the air in the rooms housing the optics and detector lead to variations in X-ray transmission with temperature, pressure and humidity, especially below ~ 10 keV. These variations are accounted for in modeling the response function, but the size of the correction can be substantially suppressed by the frequent X-ray source intensity measurements, as well as constant monitoring of temperature, pressure and humidity in order to do model interpolation between the through X-ray beam measurements.

A key aspect of the low-energy calibration is the use of a Silicon detector for measuring the effective area below ~ 12 keV. The Si detector has very low fluorescence compared to Ge, due to its low Z. In addition the fluorescence X-rays are very low energy, and thus the detector redistribution of incident X-rays is minimized. For the low energy effective area different X-ray source operating parameters are also utilized. In particular the X-ray source voltage is lowered; this markedly reduces higher energy X-ray production and associated scatter and fluorescence, which would otherwise increase the detector energy redistribution.

As mentioned above, the use of 20 multilayer subgroups permits constraining the multilayer parameters in a more refined fashion by limiting analysis of any effective area data to reflections off of identical multilayer coating sets. The subdivision of each multilayer coating group in half suppresses finite X-ray source distance and size effects.

All the above techniques provide better control of the above-mentioned systematics, as reflected in many of the terms in the error budget presented below.

Error Budget Description

The errors in the effective area determination can be divided into 4 broad categories; statistics; X-ray beam; detectors and electronics; optics.

The “statistics” category includes Poisson errors, background subtraction errors and detector redistribution errors. The latter result from the statistical fluctuations generated in rediagonalizing the detector response matrix from X-ray throughput measurements.

The second class of errors involves the X-ray source and the beamline. The X-ray source contributes uncertainty through temporal fluctuations in intensity and spectral stability. There are also errors associated with the beamline, including window uniformity and the finite size of the beam (and associated divergence effects). The accuracy with which the beam spectrum can be parameterized produces a systematic uncertainty. An important class of errors is due to the environmental stability of the X-ray beam. This pertains to the variation in X-ray transmission

through the beamline due to variations in optical depth due to pressure, temperature and humidity fluctuations.

The third class of errors involves the X-ray detector and electronics. There are fitting errors associated with finite detector energy resolution, drifts in electronics gain due to temperature effects and energy offset errors due to non-linearity in the electronics and detector. Count rate errors are introduced because of detector window non-uniformity and deadtime and pileup errors in the electronics. Of these errors, deadtime and pileup corrections are small, as are un-corrected gain variations. The dominant errors are associated with the accuracy of knowledge of the resolution kernal and off-diagonal elements in the response.

The optics errors are primarily associated with geometric effects such as the finite source-optics distance leading to both beam divergence and incomplete illumination of the upper conic section of the optics. This results in a systematic error associated with the incomplete sampling of the effective area. Angular alignment errors, resulting in an imprecise knowledge of in and out of plane incidence angles are included in this category.

All the above errors were estimated using a variety of approaches. In some cases, such as detector redistribution errors, modeling was utilized. X-ray source stability was directly measured, as were errors associated with transmission, whether of windows or those associated with environmental effects. Indeed these measurements were used to determine the maximum tolerable integration time on the optic between X-ray through beam measurements. Errors associated with the X-ray source spectrum were determined by direct fitting of X-ray through beam data using a parameterized model for the spectrum. The detector errors were determined by direct measurement, and the electronics errors either through direct measurement (e.g. deadtime) or through calculation based on manufacturer's specifications (e.g. gain drifts, non-linearity etc., pileup rejection etc.). The table below is reproduced from Appendix B, which describes each of these measurements in more detail.

	Detector & X-ray Source Setting	Si	Si	Si+Ge_M	Ge_M+Ge_H	Ge_H
	Energy Range [keV]	6-8	8-12	12-25	25-55	55-78
1	Statistics	0.7%	0.7%	0.8%	0.7%	0.8%
2	X-ray Beam	2.1%	1.6%	0.8%	0.6%	0.8%
3	Detector & Electronics	0.7%	1.0%	0.8%	0.7%	1.0%
4	Optics	1.8%	1.8%	2.2%	2.1%	1.8%
	Total	**2.9%**	**2.7%**	**2.7%**	**2.7%**	**2.6%**
1	**Statistical**					
1.1	Measured Event Statistics	0.7%	0.7%	0.7%	0.7%	0.7%
1.2	Fitting Error: Detector Response Function Spectral Deconvolution	0.05%	0.05%	0.3%	0.2%	0.2%
1.3	Ambient Background Subtraction	0.05%	0.05%	0.05%	0.05%	0.2%
2	**X-ray Beam**					
	Beamline Window Uniformity	1.0%	0.5%	0.2%	0.2%	0.2%

2.1						
2.2	X-ray (Io) Source Spectral Stability	0.00%	0.00%	0.04%	0.18%	0.33%
2.3	X-ray (Io) Source Spatial Uniformity over Aperture	0.0%	0.0%	0.0%	0.0%	0.0%
2.4	Residual Error in X-ray throughput after Correction for Temp/Pressure/Humidity	1.5%	1.0%	0.5%	0.2%	0.2%
2.5	X-ray (Io) Beam Spectrum Model	0.2%	0.5%	0.2%	0.2%	0.5%
2.6	Finite Beam Size (including scatter throughout beamline)	1.0%	1.0%	0.5%	0.5%	0.5%
3	**Detector**					
3.1	Detector Electronics Energy Scale Integral Non-linearity	0.02%	0.41%	0.27%	0.18%	0.20%
3.2	Detector Energy Scale Integral Non-linearity	0.02%	0.41%	0.27%	0.18%	0.20%
3.3	Gain Drift between I and Io measurement	0.00%	0.00%	0.00%	0.00%	0.00%
3.4	Fitting Error Due to Finite Detector Energy Resolution	0.2%	0.5%	0.2%	0.2%	0.5%
3.5	Fitting Error due to Environmental Drift in Detector Energy Resolution	0.1%	0.2%	0.1%	0.1%	0.2%
3.6	Detector Response Function Systematic Error	0.1%	0.1%	0.2%	0.1%	0.1%
3.7	Detector Uniformity (including detector window)	0.2%	0.2%	0.2%	0.2%	0.5%
3.8	Deadtime Correction Uncertainty	0.3%	0.3%	0.3%	0.3%	0.3%
3.9	Pileup Correction Uncertainty	0.5%	0.5%	0.5%	0.5%	0.5%
4	**Optics**					
4.1	Optic Angular Alignment Uncertainty	1.0%	1.0%	1.0%	1.5%	1.5%
4.2	Optic Horizontal & Vertical Alignment -- combine with above	0.2%	0.2%	0.2%	0.2%	0.2%
4.3	Detector aperture Size Uncertainty	0.2%	0.2%	0.2%	0.2%	0.2%
4.4	Measurement Sampling/Addition	1.5%	1.5%	2.0%	1.5%	1.0%
4.5	Finite Distance Response Model	0.3%	0.3%	0.5%	1.0%	1.0%

1.1: total event statistics before detector response correction and background subtraction
1.2: statistical error in correcting (or alternatively fitting) the off-diagonal detector response; assumes known form for response function (see section 3)
1.3: measured ambient background ~0.1 cnts/sec/keV in calibration facility

2.1: Uncertainty in uniformity of beam windows under constant environmental conditions (includes thickness variation and bowing under vacuum)
2.2: Source spectral variation for a nominal 3C temperature change (Voltage Temp drift = 80 ppm/C, Current Temp drift = 50 ppm/C)
2.3: Uniformity of beam over aperture (or systematics in any necessary correction), under constant environmental conditions -- the X-ray source itself is expected to be perfectly uniform over the full optic aperture
2.4: Residual error in X-ray throughput after correcting for T,P,humidity
2.5: Contribution of W peak complexes in the 8-11 and 55-70 keV range to uncertainty in the (otherwise) smooth source spectrum model
2.6: Spot size = 3x5 mm, also includes scatter in air/windows which is simulated to be small -- only
3.1: DE = 0.05 keV (dA/dE*DE < 1.0%) -- Maximum deviation = integral non-linearity in energy calibration in the energy bands -- Canberra 2020 spec <+- 0.05% for 2 us shaping
3.2: DE = 0.05 keV (dA/dE*DE < 1.0%) -- Maximum deviation = integral non-linearity in energy calibration in the energy bands -- get from Brian
3.3: I and Io measurements performed close together in time
3.4: $\Delta E \sim 1$ keV for Ge & ~0.2 keV for Si (for I/Io decovolution)
3.5: $d\Delta E = 5\%$ peak width uncertainty (for I/Io decovolution)
3.6: Compton + K escape (for I/Io decovolution)
3.7: Relative Q.E. and attenuation uniformity of direct vs focused spot size
3.8: Deadtime measured directly from electronics signal and pulser scheme
3.9: Residual pileup error in pile up rejection channel of TC244 spec amp
4.1: Assume ~4" misalignment
4.2: Changes position on detector
4.3: Sample more/less of PSF
4.4: Systematics in aperture size/alignment on optic & incomplete optic sampling
4.5: Correct for beam divergence (estimated from raytrace simulation)

4.2 Focal Plane

This section describes the plan for the calibration of the Cadmium Zinc Telluride (CZT) focal plane hybrid detectors for the NuSTAR satellite. The candidate flight units are selected from CZT-ASIC hybrids following screening to confirm that the detectors meet the performance requirements. Calibration measurements will be undertaken for all of the flight hybrids (8) as well for the flight spares (4).

ASIC-CZT hybrids (hereafter "hybrids") are designated as H21, H22, etc. The identification of all of the components (e.g. CZT detector, ASIC die, and ASIC wafer identifier, etc) is maintained via the Kadmos database at Caltech: http://kadmos.caltech.edu. In total, there will be 8 flight detectors and 4 flight spares fully calibrated.

4.2.1 Calibration requirements

The quantum efficiency of each focal plane hybrid detector pixel shall be determined to 5% accuracy between 6 keV and 80 keV during ground calibration.

Rationale : Required to meet the absolute flux knowledge requirement.
Controller : Instrument Manager
ID : L4-FPE-139

The photopeak efficiency shall be determined for each focal plane hybrid detector pixel to an accuracy of 3% between 6 keV and 80 keV during ground calibration.

Rationale : Required to meet the absolute flux knowledge requirement.
Controller : Instrument Manager
ID : L4-FPE-140

The transparency of the focal plane entrance window shall be determined to 0.5% accuracy between 6 and 80 keV.
Rationale : Required to meet the absolute flux knowledge requirement.
Controller : Instrument Manager
ID : L4-FPE-141

The uncertainty in the position bias correction in the measurement of the x-ray interaction relative to a physical detector coordinate system shall be less than 100 microns anywhere on the active area.
Context : This is the systematic part of the positioning due to detector distortions.
Rationale : This requirement is derived from the source positioning requirement.
Controller : Principal Investigator
ID : L4-FPE-65

The focal plane/electronics system shall measure the absolute energy of an X-ray to better than 0.5 keV (3-sigma) from 10-60 keV.
Rationale : This requirement is derived from the line centroiding requirement.
Controller : Principal Investigator
ID : L4-FPE-201

4.2.2 Hybrid Calibration Approach

The calibration of the focal plane detectors involves determining the response of pixels (gain, position, quantum efficiency) at fixed energies as well as developing a model of the detector response to interpolate over the entire NuSTAR energy band. All of the data that we will take will be used to define a model of the CZT response. Here we present an overview of the focal plane calibration effort. Details of the individual measurements may be found in Appendix C.

There are five principal aspects of the focal plane detector calibration:

1) *Determine pixel-to-pixel gain variations as a function of high voltage and temperature*

   There are significant gain variations (up to 10%) between pixels that may vary as a function of high voltage and temperature. In addition, about 20 - 40% of events (depending on energy) have charge split among multiple pixels and, depending on how the charge is split, a different gain correction may be required. There are 13 dominant topologies (called "grades", see below) for sharing charge between a pixel and its eight neighbors, each of which may require a different gain correction. This calibration is required to meet spectral resolution and absolute energy measurement requirements.

2) *Determine response matrix for each pixel*

   The response of individual pixels may vary based on charge transport properties that vary pixel-to-pixel. The shape of the photopeak and the tailing in the detector is strongly dependent on energy and will also depend on temperature, bias voltage, and event topology. Determining the response as a function of energy for the range of operating conditions expected on-orbit is required to meet the requirement on knowledge of the photopeak fraction.

3) *Determine pixel centroids and areas*

   The active area of each pixel is determined by non-uniform internal electric fields in the CZT. This produces pixel-to-pixel size and shape variations. The area of each pixel must be determined to distinguish variations in pixel quantum efficiency from variations in pixel size. To meet source position requirements, the pixel centroids must be determined to better

than 100 microns (3-sigma).

4) *Determine quantum efficiency of each pixel*

   The quantum efficiency must be determined for each pixel as a function of energy. As noted above pixel QE variations must be separated from size variations.

5) *Determine relative position of hybrids on the flight focal plane.*
   Once the four hybrids are placed on the flight motherboard the relative positions must be determined to better than 100 microns (3-sigma).

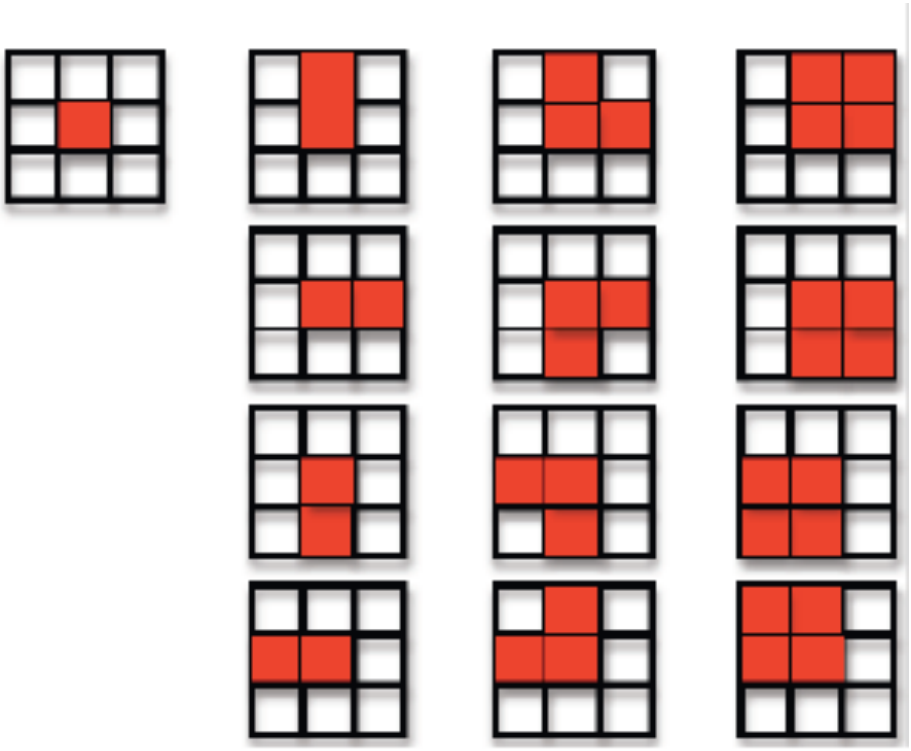

Figure 3 Possible event topologies due to charge sharing between pixels. 61% of events are Single-Pixel (Grade 0), 33% are Double-Pixel, and 5% are either Triple- or Quadruple-Pixel events. First column, grade 0; second column (top to bottom), grade 1 – 4; third Column, grade 5 – 8; fourth Column, grade 9 – 12.

4.2.3 Measurements - Hybrid Flood Illumination

Experimental Setup

The hybrids are placed on a flight-like motherboard and MISC (controller board) in an insulated box that is thermally controlled to better than 1^{o} C by a computer-controlled forced air unit. The source is secured above the detector with a minimal amount of thermal insulation and a thin mylar window intervening. The MISC is interfaced to a Sun workstation operating ITOS. The setup has been used for the screening of more than 30 hybrids and its operation and integrity of the data acquisition has been thoroughly verified. The throughput of the system is limited by the readout

electronics (see Appendix A) so that the maximum practically achievable throughput is ~300 counts per second.

Measurement Strategy

There are three primary measurements that we will undertake with the flood illumination data. The following table outlines the integration times for all of the measurements, with the enumerated list below giving the details of each of the sets of measurements.

Source	Integration Time	HV Bias	Temperature
Determination of Pixel Gain for all Grades			
^{241}Am	48 hours	Ideal for the hybrid	Ideal for the hybrid
Determination of Temperature Dependence of Gain.			
^{241}Am	24 hours	Ideal for hybrid	Scanned from 10 – 0 °C in 0.1 °C steps
Determination of Model Parameters ($\mu\tau$ electron & hole per pixel)			
^{241}Am	36 hours	12 Hours each at -300, -400, and -500 V	Ideal
^{57}Co	48 hours	Ideal	Ideal
^{155}Eu	24 hours	Ideal	Ideal
Total Time	180 hours		

Determination of Pixel Gain for all Grades

For this measurement the hybrid is maintained at the nominal operating temperature and bias voltage and flood illuminated with a ^{241}Am source. The 13.9 and 59.6 keV lines will be used to determine the gain for all grades. For the ^{241}Am source, roughly half of the counts fall in the 59.6 keV line while about 13% of the counts fall in the 13.9 keV line. Assuming an overall throughput of 300 counts per second, this corresponds to a throughput of 150 counts per second in the 60 keV line and about 40 counts per second in the 13.9 keV line. Of these, 2% will be quadruple-Pixel (Grade 9 – 12) events, so the limiting rate per pixel is roughly 7.6×10^{-4} counts per second in the 13.9 keV line, or 65 counts in 48 hours of integration.

The requirement on the gain determination is that we identify the energy of an individual photon to

better than 0.5 keV. At 13.9 keV, we take the average energy resolution of a CZT detector to be 400 eV (FWHM). The uncertainty in the gain determination then is this factor multiplied by the statistics uncertainty in the measurement. The table below described the uncertainties of the various topologies. In all cases we meet the requirement.

Event Topology	Counts / Pixel / Line / Grade	ΔE / SNR (keV)
Single Pixel (Grade 0) (61%)	2.7×10^3	0.015
Double Pixel (Grades 1-4) (33%)	365	0.042
Triple Pixel (Grades 5 – 8) (3%)	33	0.138
Quadruple Pixel (Grades 9 – 12) (2%)	22	0.170

Gain Dependence on Temperature

For this measurement the hybrid is illuminated with an ^{241}Am source. The bias voltage is maintained at the nominal operating point for the hybrid. The temperature is stepped from 10 to 0 degrees in 0.1 degree steps every 14 minutes. In each interval we should collect ~24 grade 0 counts per pixel in the 13.9 keV line and 87 grade 0 counts per pixel in the 59.6 keV line. Using these data we will determine the temperature dependence of the gain. Grade 1 – 4 59.6 keV gamma-rays will be used to check whether all grades share the same gain dependence. If necessary, multiple steps will be combined to improve statistics.

Determine Model Parameters

Our model of the detector response includes the charge transport inside the CZT. To determine the charge transport parameters in our model we conduct the following measurements

1. *Bias scans to determine $\mu\tau_e$*
   For this measurement the hybrid is illuminated with an ^{241}Am source. The temperature is maintained at the nominal operating point for the hybrid and flood data are taken at bias voltages of -300, -400, and -500 Volts. The shift in the 60 keV line is then used to determine the $\mu\tau_e$ for each pixel. The 12 hour integrations should provide several thousand Grade 0 counts per pixel in the 59.6 keV line, which is more than enough to determine the photopeak location used to determine $\mu\tau_e$.
2. *Energy vs. depth measurements to determine $\mu\tau_h$*
   For this measurement the hybrid is maintained at the nominal operating temperature and bias voltage and illuminated with a ^{155}Eu source and then a ^{57}Co source, with only grade 0 events considered. We will use the 86.5 and 105 keV lines from the ^{155}Eu and the 122 keV line from the ^{57}Co. The high-energy lines from these sources produce photons that penetrate further into the detector than the 59.6 keV line from the ^{241}Am source. For these sources there is a "depth" tailing effect that can used to determine the ratio of $\mu\tau_e$ to $\mu\tau_h$ for the pixel. Since we will already have determined $\mu\tau_e$, we will use these data and

simulations of the charge transport inside the CZT to determine $\mu\tau_h$ for each pixel independently.

4.2.4 Measurements - Fine beam scanning

Experimental Setup

Detector and data acquisition. The detectors are mounted on a flight-like motherboard inside a cold box. The cold box is maintained at the optimal operating temperature for the hybrids (which is determined during hybrid screening, but is nominally between 0 and 10 degrees C) under a nitrogen purge.

The motherboard is connected to a focal plane electronics board that reads out the ASICs and transmits the data to the laboratory computer. The key elements of data acquisition system are similar to the one used on-orbit – an engineering test unit of the focal plane MISC board, and flight-like motherboards are used. The throughput of events is limited to <400 counts per second. However, the electronics monitor the live time to better than a microsecond, so the incident rate can be up to 10^4 cps before pileup and live time uncertainties become an issue (see Appendix A for details).

The entire setup is mounted on a set of translation stages that allow movement in both the X- and Y- directions. The stages have a full-range 50 mm, with an accuracy of 1 micron in both stages.

X-ray Generator. The X-ray generator is a Rigaku 3 kW generator that can be operated at voltages from 20-60 kV, with currents from 2-50 mA. The primary source is a Mo tube, with K-alpha and K-beta lines at 17.4 and 19.6 keV respectively, and a Bremsstrahlung continuum (see Figure). The relevant features are an intense beam (enabling count rates of > 10^4 in a 100 micron x 100 micron slit) and high stability of 0.01%.

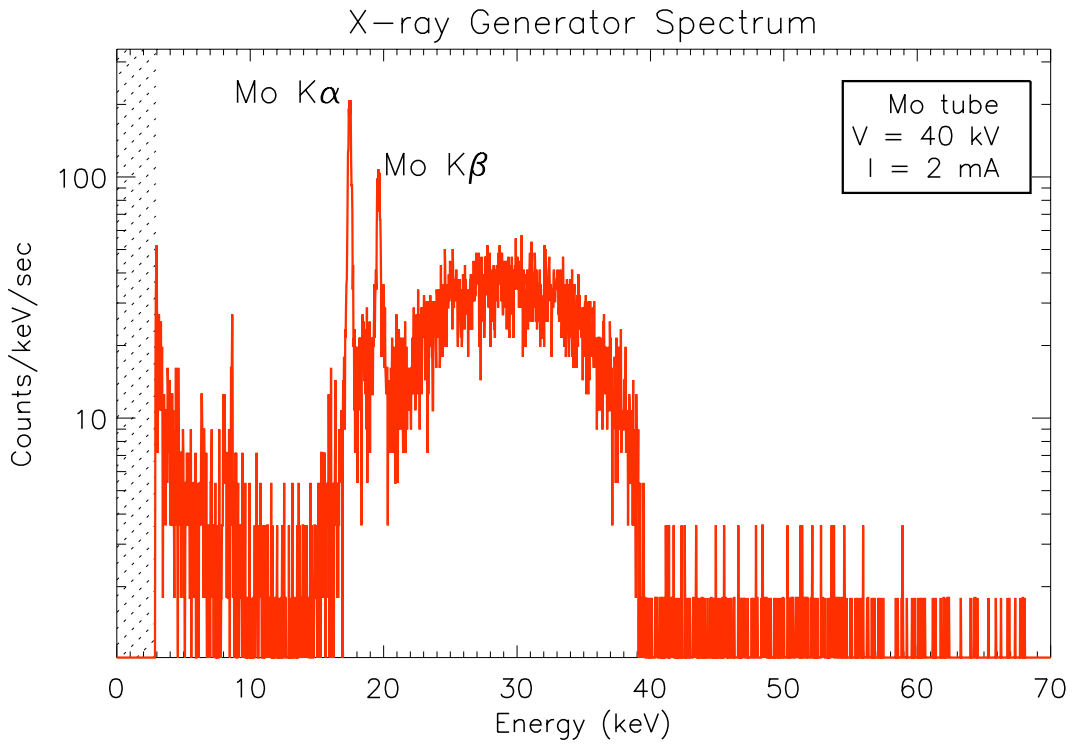

Figure 4 Spectrum from the XRG with V=40 kV, I=2ma, Al filter of 2.3mm to reduce count rate (slit = 50 microns). Integration time was 20 s, spectrum is live time corrected with net count rate of 700 cps. The spectrum was taken with a Silicon detector and is not corrected for its response.

Scanning stage and reference coordinates. All of the positional data from this scan are measured in relative "stage coordinates" from the X/Y translation stage, which has a positional accuracy of 1 micron in both directions. The position of the X-Y stage is read out every 30 milliseconds so that the individual X-rays recorded by the DAQ are collated with a specific X/Y stage position.

It should be noted that the detectors are rotated with respect to each other on the motherboard so that the critical corner for a detector in position A is in the top left corner. Detectors in positions B, C, and D are rotated by 90, 180, and 270 degrees clockwise from the detector in position A.

The Z-axis is measured from a plane parallel to the surface of the CZT detectors, with the positive direction oriented towards the X-ray beam. We adopt a right-handed coordinate system with the Y-axis defined positive toward the ceiling.

Measurement Strategy

There are several goals of the fine-beam scans. These goals will be achieved through two scans of each hybrid. The settings of the XRG and the integration time for each scan are given in the table below:

XRG Setup	Integration Time	HV Bias	Temperature
Determination of pixel centroids and pixel boundaries			
60 kV, max throughput* (May use Al filter)	1 Day	Ideal	Ideal
Low-energy Response			
20 kV, max throughput	1 Day	Ideal	Ideal

The data from these two scans will be used to provide the following information:

1. *Determine the relative position of each pixel*
   These data will later be combined with the absolute positions measured by a hole-plate (see below) to satisfy the centroiding requirement.
2. *Determine the size and shape of each pixel*
   Though the readout ASIC is set on a regular grid, the active region of each pixel is determined by the internal electric field in the CZT. This field is affected by irregularities and impurities in the crystal, which means that the active area of each pixel can only be determined by incident X-rays.
3. *Determine the response of each pixel to continuum emission*
   We will develop a model of the detector response and the internal charge transport based on the flood illumination of the detector with radioactive sources (see above). Based on the measurement of the incident spectrum from the XRG we will check our model of the detector response by confirming that it reproduces the observed spectrum when the hybrid is illuminated with a continuum source. This will be done at high energies with the 60 kV scan. The 20 kV scan will be used to check the low-energy response of the detectors.
4. *Determine the relative quantum efficiency for each pixel*
   Since the beam is stable, we can determine the relative quantum efficiency for each of the pixels.

Scan Strategy

The projected beam size is square, 50 x 100 microns. The incident count rate is several thousand/second, so that a measured count rate of ~350/s through the acquisition system is easy to achieve (in fact Al filters must be used to reduce the incident count rate). We performed

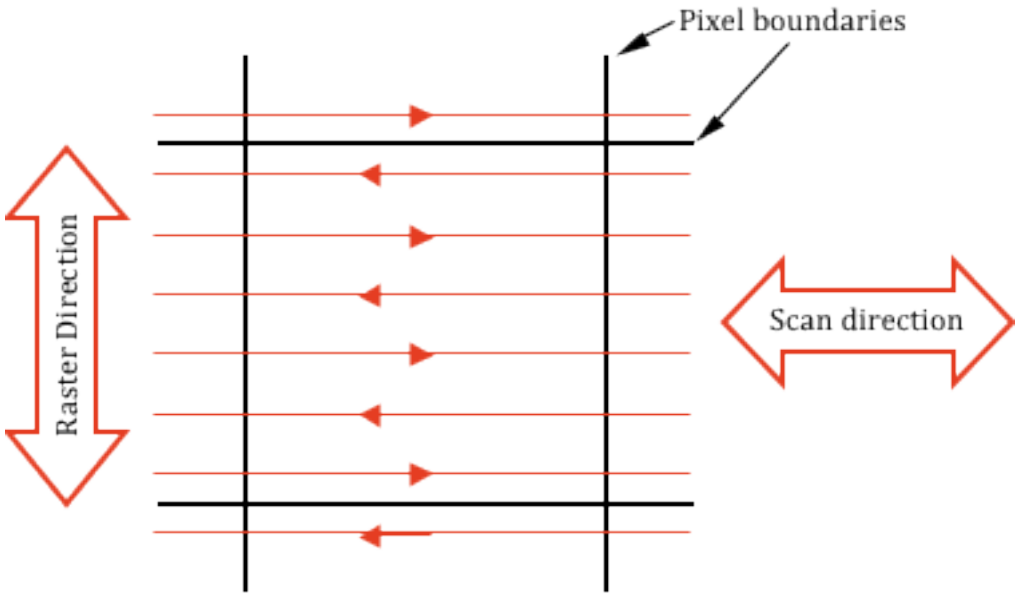

Figure 5 Scan pattern

simulations (described below) using a worst-case 100 micron slit to be conservative. The final slit size will be chosen after further testing to determine optimal power settings on the generator.

We do not require that the slit scanning direction be accurately aligned with any feature on the detector. Rather, we will begin scanning just off the edge of the detector. There may be a rotation of several degrees between the X-direction of the scan and the line connecting the X-centroids of the pixels. The scan will commence in the X-direction (of the stages) at a rate of 100 microns/sec until the entire detector width is covered, then will step up in the Y-direction by 100 microns and traverse back in the X-direction, so that each pixel is covered by 6 scans in the X-direction at Y-positions differing by 100 microns. Then, the same pattern will be repeated but scanning in the Y-direction and stepping in X. The total time taken to complete this scan is 11.5 hours per dimension, or 23 hours total.

Error Budget Analysis

In order to determine the accuracy of centroid and pixel size measurements, we performed simulations given the scan pattern over a range of count rates. The simulations correspond to scanning the detector edge-to-edge with a Gaussian beam with 100 micron FWHM (which represents the worst case of a 100 micron square slit broadened due to scattering), being shifted by 100 microns for each scan. Thus, each point on the detector is crossed once in the X-direction and once in the Y-direction. This is a worst-case analysis, since this is the maximum slit size, and a narrower slit will improve the errors.

The results shown here relate to scanning the edge of a single pixel at a count rate of 300 counts/sec. The edge is scanned six times, and each event is associated with a pixel based on where the photon lands based on the pixel with the maximum registered pulse height. For fitting the data and reconstructing the edge, the only information available is position of the stages as a function of time, and the pixel event data as a function of time.

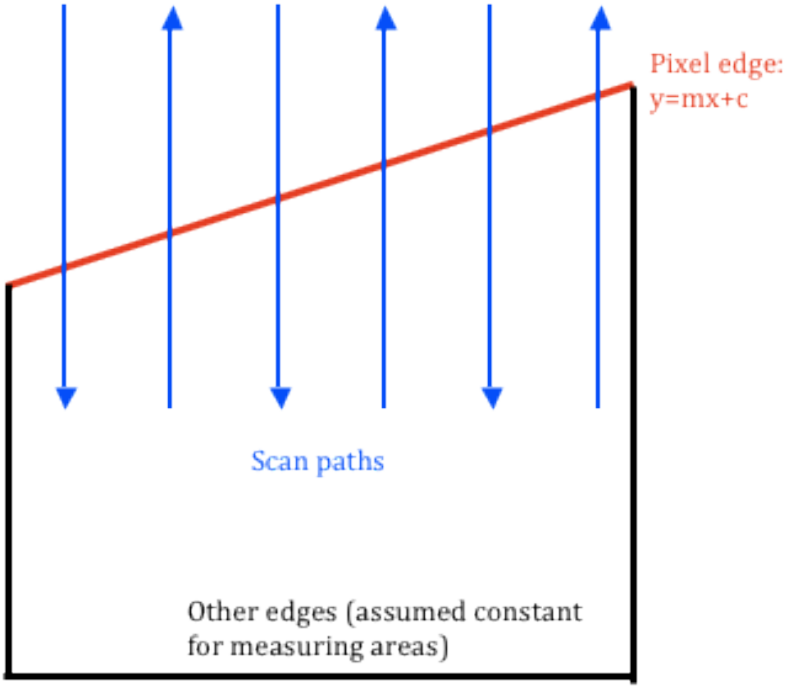

We simulated 1000 fits, with the edge given by y=mx+c, and scanning in the y direction. The slope 'm' was randomly selected in the range +-5 degrees (+-0.08 radians). The offset 'c' was randomly selected in the range +- 100 microns. With 6 scans across the edge, the pixel edge can be recovered to better than 14 microns, and angles can be recovered to better than 2.5 degrees. If we assume that we have measured the other 3 edge accurately, then we can determine areas to better than about 1.5

Count rate: Maintaining a scan rate of 100 microns/second, we changed the count rate to the following values. This table lists the uncertainties in area, slope and offset, such that 99% pixels have lower errors than the value quoted in the table.

Count rate	Area uncertainty	Offset uncertainty	Slope uncertainty
10 counts/sec	7.2%	94 microns	0.280 (15.6^{o})
30 counts/sec	3.4%	34 microns	0.090 (5.1^{o})
100 counts/sec	1.4%	14 microns	0.045 (2.6^{o})
300 counts/sec	1.2%	8 microns	0.025 (1.4^{o})
500 counts/sec	0.6%	6 microns	0.015 (0.9^{o})

In another simulation, we allowed individual edge angles to vary up to +- 20 degrees, at a count rate of 100 counts/sec. Even in this case, the pixel areas can be recovered to better than 1.4% for 99% of the pixels. The edge offsets can be measured to better than 14 microns, and slopes are measured to better than 0.03 (~2^{o}).

The total error in area contains contributions from uncertainty in all 4 pixel edges, and Poisson variability in the counts from the X-ray generator. The total error is estimated to be less than 3% (99% confidence interval) by combining these terms. The analysis of the simulated data is a first-pass analysis using basic fitting procedure. For actual data, we will use more detailed fitting methods and get smaller errors in the final parameters.

Summary

We conclude that for the worst-case slit size and count rate we can still meet the requirement for pixel area measurement and exceed by more than a factor of three the centroid measurement requirement. The expected count rate is 350 counts/sec, and the slit size < 100 microns, so that we expect the area uncertainty to be < 3% and the pixel centroid determination < 10 microns (compared to the 100 micron requirement).

4.2.5 Limited aperture illumination for quantum efficiency

In this set of measurements, aimed at measuring the absolute quantum efficiency and photopeak efficiency of the detector, calibrated radioactive sources will be masked with a set of tungsten slits to illuminate an area of the detector. The masked radioactive sources have all been previously calibrated against reference Ge and Si detectors. The setup is designed to achieve accurate source to detector knowledge. This allows us to produce a mass model of the masked calibration source in GEANT4 and predict the rate of photons incident on the surface of the detector. By comparing the integrated count rate with the predicted rate form our simulations we can compute the bulk quantum efficiency for the illuminated region.

Experimental Setup

Detector Mounting and Data Acquisition

This measurement will use the same thermally controlled cold box and the X/Y stage from the XRG setup used to measure the pixel centroids. As before, the cold box will be mounted on the X/Y stage so that the entire focal plane may be scanned with the radioactive sources without having the manually reposition the cold box.

This setup is translated away from the XRG beam pipe to allow for the calibration source holder to be mounted on the beam pipe. As before, the source is held stable while the cold box is scanned past the X-ray mask.

Description of Radioactive Source Setup

The calibration sources will each be placed in a source holder that extends off the end of the XRG beam pipe. The sources will be positioned in the source holder so that the nominal distance between the source and the X-ray mask is at least 5 cm. Each source is packaged slightly differently, so the distance between the source and the mask will vary for each source. Once the source is in place the distance between the source and the mask will be measured to an accuracy of 25 microns.

The tungsten slits are chosen to be 1.27 mm thick so that they will stop at least 99% of the highest energy X-rays in our sources. They are spaced to provide a square aperture with sides of 5 mm. This spacing was chosen to produce a 1% fractional uncertainty in the area of the aperture assuming a nominal uncertainty in each side of 25 microns.

As before, the "minimum safe" slit-to-detector distance is roughly 2.5 cm. Treating the radioactive source as a point source, this produces a projected illuminated region of 0.72 x 0.72 cm on the detector surface (roughly illuminating 144 pixels).

Description of Calibration Sources

All of the sources are calibrated using several reference detectors (two Ge detectors, and one Si detector). The sources, the lines that we expect to use, and the activity as measured by each reference detector, are given in the table below. The source activity given represents our estimation of the source activity.

Source	Lines	CIT GE Estimated Activity	RHESSI Flight Spare Ge Estimated Activity
^{55}Fe	5.9	7.91 +/- 0.2 uCi (TBC)	6.84 +/- 0.3 uCi
^{241}Am	59.6, 13.76+13.95	3.644 +/- 0.010 uCi	3.651 +/ 0.009 uCi
^{155}Eu	86.5, 105.3	10.73 +/- 0.02 uCi	10.81 +/- 0.02 uCi

Once the sources are mounted in the calibration setup, the entire apparatus will be calibrated using the RHESSI flight spare Ge detector and a Si detector. A GEANT4 mass model of each source and its holder will be constructed to determine the absolute flux observed by the Ge and/or Si detector. As can be seen in the table above, our previous attempts to cross-calibrate the absolute activity of a radioactive source between Ge detectors have yielded results that agree to better than 1% for the ^{241}Am and ^{155}Eu sources, while the Si detector will be used to calibrate the ^{55}Fe since there are discrepancies between the response of the Ge reference detectors at low energies due to uncertainties in window and dead layer thicknesses.

Measurement Strategy

Source (lines)	Integration Time	HV Bias	Temperature
^{241}Am (59.6, 13.9 keV)	1 Day	Ideal	Ideal
^{155}Eu (86.5 keV)	1 Day	Ideal	Ideal
^{55}Fe (6 keV)	1 Day	Ideal	Ideal
Total Time	3 Days		

The hybrids will be mounted in an identical manner as for the XRG scan. If possible, this measurement will directly follow the XRG measurement so that the hybrids need not be removed from the cold box. The cold box is installed on the translation stages, with the stages arranged so that the full range of the translation stages allows for scanning of all detectors without repositioning the cold box.

Each detector will be scanned with each source, with the same steps included in each scan. Since all four detectors share the same readout electronics (and limiting throughput), only the detector being scanned will be read out.

1) The detector is moved so that the illuminated region is near the critical edge of the detector.
2) An observation is taken with duration such that the expected number of counts in the weakest gamma ray line to be used results in a statistical uncertainty of roughly 0.5% in each aperture region. This duration will vary source by source.
3) The detector is moved [360 microns] (TBD) in the horizontal direction and another integration is taken. This process continues until an entire horizontal strip of the detector has been observed.
4) The detector is then returned to the initial position, translated vertically by [360 microns] and the horizontal scan is performed again. This process is repeated until the detector has been completely sampled.

Simulation of Scans

Preliminary GEANT4 simulations using the calibrated ^{241}Am source and a source-to-slit distance of 5 cm and a square mask with sides of 5 mm were performed to estimate the count rate at the surface of the CZT. As the final experimental setup is refined, the simulation will be refined to match the final configuration of the calibration setup. A schematic of the source geometry is shown below along with the prediction of the count rate at the surface of the CZT.

For this source geometry, the integrated rate at the surface of the CZT is 63.8 counts per second. Assuming the nominal non-paralyzable deadtime of 2.5 ms per count, this results in a total throughput of 55.17 counts per second and throughputs of 26.2 counts per second in the 59.6 keV line and 6.62 counts per second in the 13.9 keV line.

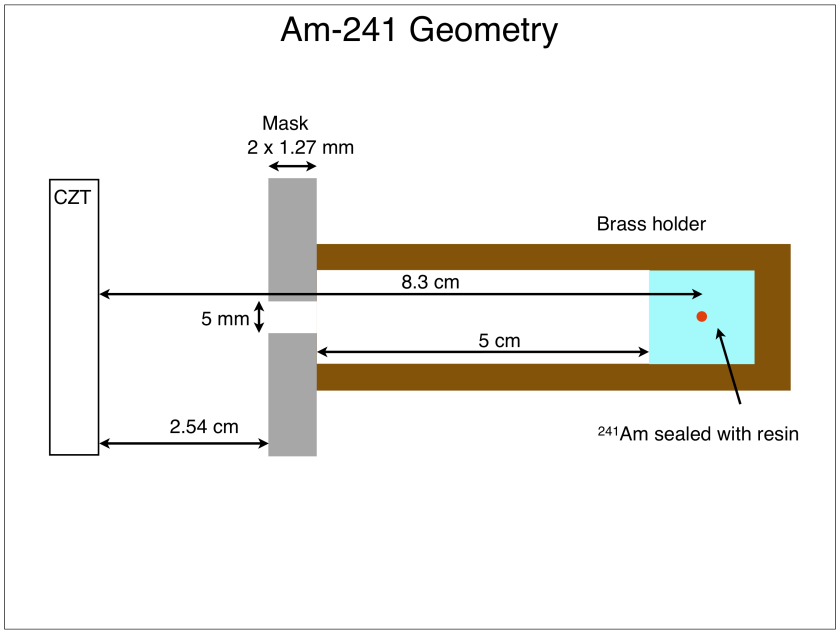

Figure 6: Schematic of source geometry for limited aperture illumination.

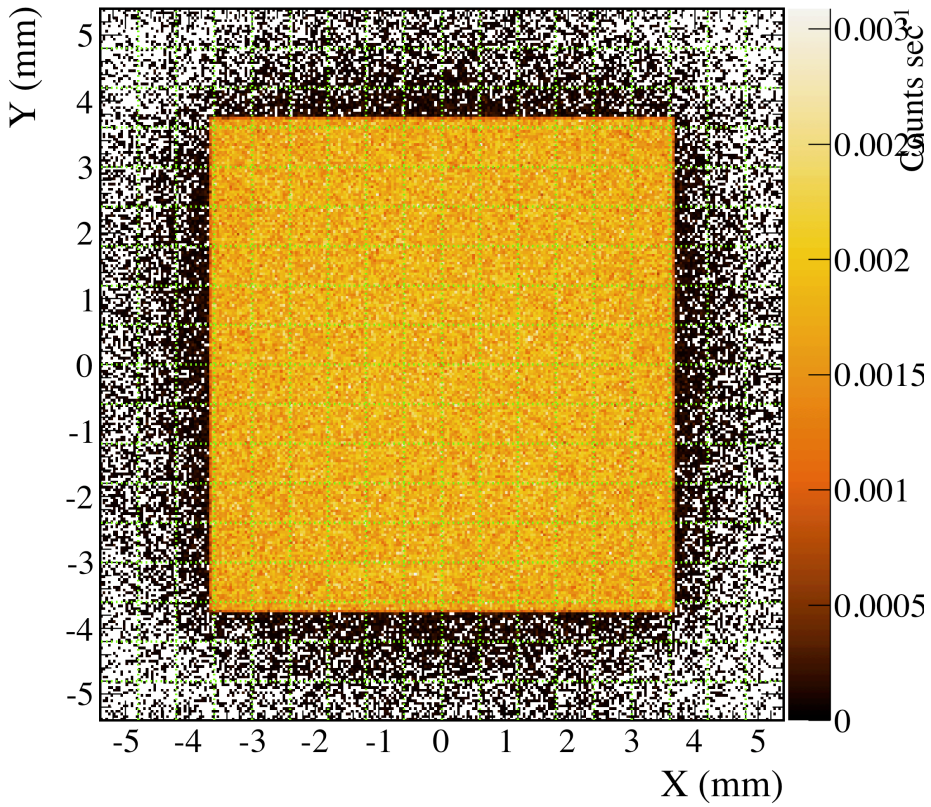

Figure 7: Intensity map for photons incident on the surface of the CZT

Quantum Efficiency Error Budget

Source	Contribution to Q.E. Measurement	Running Total
Statistics	0.5%	0.5 %
Calibration Source Geometry and Activity		
Mask Aperture Area	1.41 %	
Calibration Source Activity	1.0 %	
Source-to-slit distance	1.41 %	
Subtotal	2.24 %	2.29 %
Photopeak Efficiency	2.0 %	3.04 %
Residual Uncertainties	3.7 % (max allowed)	5 %
	Total	5 %

Statistics

We have made the decision to allocate 0.5% uncertainty due to Poisson fluctuations in the counting statistics, or at least 40,000 counts in the lines of interest. It is this requirement that drives the duration of the limited aperture scans. For example, for the ^{241}Am source described above, the 13.9 keV line produces 6.62 counts per second in the 144 pixel active region. This implies an integration time of at least 6042 (~ 1.6 hours) seconds per scan position to accumulate the required counting statistics, or 16 hours to fully sample the entire hybrid. The duration of the scan will vary based on the strength of the source and the fraction of counts in the line of interest. However, we do not anticipate that any of the sources will require more than a day of integration to achieve the required statistics as the simulated case is for the weakest source.

Mask Aperture Area

For an expected tolerance of 25 microns, the aperture of the mask of 5 mm x 5 mm was chosen so that its contribution to the error in the expected count rate is 1%.

Calibration Source Activities

The calibration source activities in the lines of interest for the Q.E. measurement will all be determined to better than 1% by using two reference Ge detectors and/or a reference Si detector. In general, the cross-calibration provides an estimate of better than 1% for the Am^{241} and Eu^{155} sources, and slightly worse than Fe^{55} source. All of the sources will be recalibrated once they are installed in the calibration setup using the RHESSI flight-spare Ge detector for higher energies and the Si detector for lower energies.

Distance to Source

The distance between each calibration source and the slit will be measured to 25 microns. For a nominal distance of 5 cm, this results in an uncertainty in the source-to-slit distance of 0.05%. However, the location of the active material inside of the source packaging is not necessarily known. Our previous models of the calibration source assume that the source is located at the center of the packaging. For our larger sources (for example, the Am^{241} source), the resin that contains the active material is a cylinder with a height of roughly 1 cm and a diameter of roughly 1.25 cm. Assuming an uncertainty of 0.5 cm in the position of the source introduces an unmanageable 10% uncertainty in the distance between the source and the slit. In the future, measurements will be undertaken that change the relative orientation of the source inside the packaging and should be able to constrain the location of the active material to a much higher accuracy. For now, we assume that we will be able to localize the active region to better than 0.5 mm and that the source-to-slit distance is uncertain to 1%.

Summary of Geometric Contributions

The contribution of this to the flux through the limited aperture is as follows:

$$Flux_{Mask} = Flux_{Source} \times (Area_{Mask} / Area_{Sphere})$$

where $Area_{Sphere}$ is measured from the active region of the source ($4 \pi r_{Sp}^2$) and $Area_{Mask}$ is (R_{Mask}^2). The fractional error is:

$$\sigma_{Flux} = \sqrt{(2 * \sigma_{RSph}^2 + 2 * \sigma_{RMask}^2 + \sigma_{Flux})}$$

For $\sigma_{RSph} = 1\%$, $\sigma_{RMask} = 1\%$, $\sigma_{Flux} = 1\%$, $\sigma_{Flux} = 2.24\%$

Photopeak Efficiency

As stated above, we will determine the photopeak efficiency by modifying a GEANT4 mass model of the detector for each limited aperture scan location the required accuracy of 2%.

Residual Uncertainties

Assuming that all other measurements are within the allotted tolerances, we have a 3.96 % margin to be allotted to residual uncertainties that are TBD.

Model degeneracies

There may be components of our mass model that are impossible to disentangle and contribute to the observed spectrum in identical ways. As the models are developed the estimation of the model degeneracies will be determined.

Livetime uncertainty

The CZT livetime is measured to better than 0.1% up to incident count rates of 10^4 s so livetime uncertainty is a negligible contribution to the measurement error.

4.2.6 Hole plate measurements

Experimental Setup

To measure the registration of the four hybrids relative to one another a plate with 16 apertures, 4 per detector, will be placed in a fixture mounted in front of the focal plane. Each aperture will be 0.24 x 0.24 cm. The spacing between the plate and detector will be 5 mm. A radioactive ^{241}Am source will be placed above the plate at a distance of 30 cm. The centroid of the each of the 16 apertures will be measured.

Errors

Errors arise from source geometry uncertainties, statistics, and the errors in the pixel centroid measurements, which must be used to remove the spatial distortions intrinsic to the detector.

Source	Contribution to Measurement (3-sigma)
Statistics	10 microns
Source placement (x-y)	4 microns
Pixel centroid uncertainty	25 microns
Hole plate machining accuracy	25 microns
	Total 37 microns

Even with worst-case assumptions meeting the 100 micron requirement is straightforward. To achieve an allocation of 10 microns for statistic requires less than 1000 counts/hole, achievable in 5 minutes of integration time at a count rate of 350 cps/focal plane. In reality we will integrate for longer than this. The error due to pixel centroid uncertainty assumes that the centroids are known to the 100-micron requirement, but in reality the scan strategy we are adopting will determine them to 10 microns.

4.2.7 Caveats

The calibration approach relies on the following assumptions:

1) The pixel centroids are not strongly dependent on X-ray energy. It is not possible to perform fine-beam scans at high energy (> 60 keV) due to limitations of the Caltech X-ray generator and difficulty producing a finely collimated radioactive source that will produce the requisite count rate. Some dependence is to be expected due to the larger range of interaction depths for high energies combined with material inhomogeneities, but it is assumed this dependence is small compared to the 100 micron requirement. This will be verified in detail up to 50 keV from the pencil beam scan and cross-checked up to 86 keV using flood illumination (which can constrain how much pixel sizes vary, from which limits on the centroid variations can be derived).

   In addition, we will also check this assumption by using a trufocus 125 kVp X-ray system at MSFC. This system will provide a beam with bremsstrahlung continuum emission up to 125 keV along with K lines at 59 and 67 keV from the W target. We will take a flight-spare hybrid that we have processed through all of our calibration at low energy at Caltech and determine by how much the location of the pixel centroids and/or the pixel shapes change.

2) We assume that for high energies the pixel-to-pixel quantum efficiency variations due to dead regions in the material are small compared to the required 5% accuracy. For energies < 50 keV the QE variations will be measured using the fine beam scans. For E>50 keV this will be verified by comparing pixel-to-pixel counts ratios at 60 and 86 keV from flood illumination. This assumption will also be verified at MSFC using a flight-spare detector.

4.3 Window and Optics Thermal Cover Transparency

Two beryllium windows fabricated of 99% pure Be, each nominally 50 microns thick are placed above each focal plane. The windows were purchased from Brush Wellman and are made of PF-60, which has up to 1% impurities – predominantly BeO from a thin oxide layer not to exceed 8,000 ppm. The windows may vary in thickness so that they are up to 50% thinner in the center. According to the manufacturer, the thickness variation will be uniform.

The optics thermal covers consist of a 7 micron thick polyimide coated with 1.2 microns of SiOx and 0.16 microns of Al. There is a rip-stop made of a similar polyimide film with cutouts for strength reasons. The thickness of the coatings may vary smoothly across the film by +/-3%.

Transparency measurements for the beryllium windows and optics thermal cover will be made using an ^{55}Fe source and silicon detector masked to illuminate a 3 x 3 mm region. The source will be placed so as to illuminate the detector with a count rate of about 200 cps. The windows or cover will be inserted in the beam and the change in count rate noted. In the case of the windows, each window will be mounted on a translation stage and a grid of points will be taken to map out the thickness variations. We plan a pattern of about [5 x 5 points](TDR) covering a 2.5 x 2.5 cm

area and based on the measurements will map the uniform thickness variations. Residuals will be ascribed to random thickness variations.

In the case of the optics cover, the number of measurements required across the cover is determined by the +/-3% variation in coating thickness of Al and SiOx on the polyimide substrate. The gradient is expected to be smooth. Twenty measurements will be made across three lines aligned with the center of the six sextant sections of the cover. The sampling position must be precise enough to measure both the open areas as well as the rip-stopped area. For these measurements the covers will be moved manually.

Error Budget

The measurements are designed so that statistical errors are small – we allocate 0.2% 3-sigma. This requires 4 x 10^6 counts per point, or 5.5 hours/point. In the case of the beryllium windows there will be an error due to uncertainty in the composition (ie thickness of the oxide layer). We can bound this error by comparing pure Be to the 99% pure PF-60, using maximum impurity levels listed on the Brush Wellman specification sheet. The difference at 5 keV is 0.2%, and at 6 keV it is <0.1%, so we assume this as a worst-case error. The impurities in the optics cover are not bounded by the manufacturer, but knowledge of the manufacturing process leads us to understand they are <1%, and will contribute similar errors to the beryllium windows. There will also be some uncertainty due to thickness variations that are not smooth and so not modeled by linear interpolation of points taken in the scans. These are difficult to determine from first principals or information from the manufacturer, and we assume they will be about 10% of the total uniform level of variation.

The table below provides estimates that are applicable to both the thermal cover and entrance windows.

Source	Contribution to Measurement (3-sigma)
Statistics	0.2%
Composition uncertainty	0.1% (upper limit @ 6 keV)
Random thickness variations	0.2%
Livetime uncertainty	0.13%
Total	**0.33%**

5.0 In-Flight Calibration

Note: Section 5.0 is preliminary. Simulations will be undertaken to finalize the calibration observing plan. The next draft will be distributed October 30, 2010.

5.1 Requirements on source selection

The characteristics of acceptable in-flight calibration sources are different for optical axis determination, mast adjustment, PSF characterization and absolute flux calibration. The requirements common to all measurements are that the sources must be well characterized and readily accessible to previous and existing high-energy telescopes, and sources near the Galactic Plane and Center must be avoided due to high background and source confusion.

For optical axis determination, the source must be a relatively bright, stable to better than about 5% on the timescale of 1-2 days. Either a point source or slightly extended source will work, as long as the surface flux density center is used in the analysis. There is no requirement that the source have a hard spectrum, or be detectable over the entire 6-79 keV band, although the vignetting function is steeper at high energy.

For PSF characterization, the sources must be bright enough, and have a sufficiently hard spectrum that source-dominated measurements can be made in each 5 keV interval from 6 – 79 keV. This will minimize required calibration time and reduce systematic uncertainties due to background subtraction, which are particularly important for characterizing the wings of the PSF. The targets must be point sources with a low level of spectral variability over the observation interval. Flux normalization variations can be tolerated.

For absolute flux measurements, sources must have spatial extent <~3 arcminutes in radius in order to allow for simultaneous background determination (ie the sources should not entirely fill the FOV). The sources must not be time variable, and sources near the Galactic Plane and Center must be avoided due to high background and source confusion. The spectra must be sufficiently hard to make independent measurements of spectral slope and flux individually in each 2 keV interval between 6 and 79 keV.

5.2 Calibration Target List

Source	RA (J2000)	Dec (J2000)	Purpose	Variability	Extent
3C273	12 29 06.69	+02 03 08.6	Optical axis calibration Redistribution matrix verification	1-2% on 1-day timescales	Point source with weak 20” jet
Cygnus X-1	19 58 21.68	+35 12 05.8	PSF determination	Depends on state - ~10% in hard state in 1 ks	Point source
Crab	05 34 31.97	+22 00 52.1	Absolute flux calibration Mast adjustment	33 ms pulse period	Point source in extended nebula (3-4 arcmin for E<10 keV, ~1’ E>10 keV)-

5.3 Optical Axis Adjustment and Calibration

The first calibration to be performed after instrument commissioning will be determination of the optical axis location, followed by adjustment of the telescope alignment if necessary. Two sources, 3C 273 and the Crab pulsar are appropriate for this purpose. Currently the plan is to use the Crab for mast adjustment, and subsequent to finalizing the alignment use 3C273 observations to both perform the final calibration of the location, and verify the instrument spectral response matrix.

Crab

The Crab is the primary target for the initial mast adjustment due to its high flux and stability. Using the flux at E>30 keV will minimize issues associated with the extended nature. Differencing of images made at different pulse phases (pulse 'on' minus pulse 'off') could also be used to allow the nebular emission to be subtracted so that the pulsar can be seen as a point source. Although it is close to the ecliptic, it has an ecliptic longitude that differs from 3C 273 by more than 30 degrees, so that one of these sources will be accessible at all times of year.

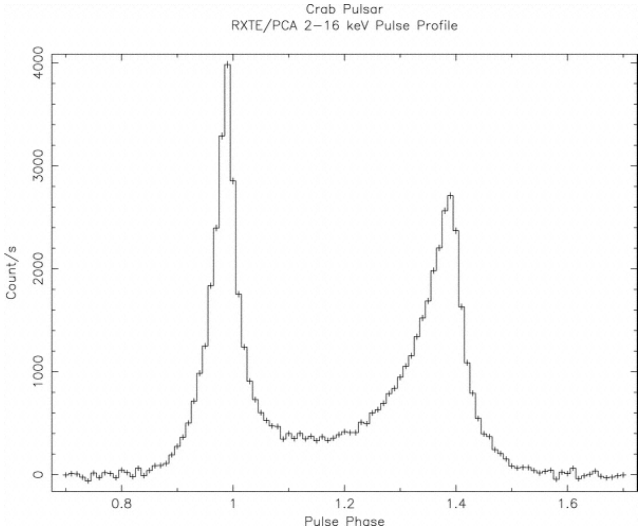

Figure 8 Crab pulsar pulse profile**.**

The pulse fraction (ratio of pulsed emission to total emission from pulsar plus nebula) depends on X-ray energy, and averages approximately 10% between 6 and 30 keV. Figure 8 shows the pulse profile as measured by RXTE (Rots et al 2004). If we take intervals of 0.15 in phase centered on the two peaks, approximately 70% of the pulsed emission will fall in the 'pulse-on' measurement (7% of the total emission). The table below shows the expected pulsar countrate in a single telescope in the pulse-on interval as a function of off axis angle (assuming 7% (TBC) of the total emission falls in the pulse-on interval). [We need to simulate what SNR we will get in 500s observation, taking into account the background fluctuations will be large due to the bright nebular emission being subtracted. We also need to simulate whether we should use the pulsar only or the total emission.]

Off axis angle (arcmin)	5 – 10 keV countrate	10 – 40 keV countrate

0	20.9	9.4
1	20.0	8.9
2	17.8	7.6
3	15.4	6.3
4	12.4	5.0
5	6.9	2.8
6	5.0	2.0

The complication with using the Crab pulsar compared to the total emission is that it requires more significant analysis that must be prepared and tested prior to launch. Because NuSTAR's absolute timing is insufficient to determine absolute phase accurately enough, the pulse phase in instrument clock time must first be determined. Then images must be binned as a function of pulse phase and differenced. This analysis is relatively straightforward to do, however the need for 'real time' results will require pre-launch testing and simulations.

A decision will be made based on simulations to be completed by December 2010 whether to use the total emission or the pulsar only.

3C273

3C 273 is a bright quasar with a jet. Chandra images show the jet extends ~20 arcseconds from the bright core (Marshall et al 2001). The jet is about 50 times fainter than the core at 10 keV. Since the jet is faint and relatively stable in flux it will not complicate the measurement, and 3C 273 can be treated as a point source. Because of the low ecliptic latitude 3C 273 will not be visible year round due to sun angle constraints.

The source flux varies on timescales of months, but by a factor less than two. We adopt the flux of Lichti et al (1995) of (2.24 +/- 0.05) x 10^{-2} ph cm^{-2} s^{-1} keV^{-1} at 1 keV with a power law spectral index of 1.6 +/- 0.01. The power law as measured by Integral in 2003 is somewhat steeper, with spectral index 1.73 +/- 0.015 (Courvoisier et al. 2003). The flux measured by Lichti appears to be close to the historical average.

Table 2 shows the count rate in a single telescope as a function of off-axis angle in two energy bands derived using Rev 0 response files. [We need to include a simulation of how well we can fit a triangular peak to find the optical axis in each telescope with ~500 - 1000 s integration per point (say 11 points from -4' to +4' in 1' steps). This would require about a 6-12 hours or so assuming 50% duty cycle.]

Off axis angle (arcmin)	5 – 10 keV countrate	10 – 40 keV countrate
0	1.53	0.82
1	1.46	0.80
2	1.30	0.65
3	1.12	0.56

4	0.90	0.437
5	0.505	0.245
6	0.364	0.179

The data analysis for 3C 273 will be straightforward. It can be treated as a point source for analysis. Standard software must be prepared prior to launch to remove quantum efficiency variations in the detector, correct for the dead space between detectors, make aspect corrected images, and extract point source fluxes.

Redistribution Matrix Cross Check

The long integrations taken on 3C273 for optical axis calibration will be used to verify the response matrix. Because 3C273 has a smooth power law spectrum, deviations in the fit to a power law near detector edges that might result from response matrix errors will be detected. The crab can also be used for this purpose (Weisskopf et al. 2010).

Point Spread Function

Note: this section will be updated when ground calibration results are available so final response matrices can be used for simulations.

Cygnus X-1 is the best candidate due to overall countrate in the high energy bands above 20 keV. Ideally it will be observed in the hard state, however given the uncertainty we plan to use energy-dependence measured from 6 to 40 keV to adjust the optics model to extrapolate to 80 keV. After completion of the ground optics calibration we will update this plan and develop an error budget based on measured energy dependence of the optics PSF and throughput.

Currently we allocate 4 days for Cyg X-1 for PSF characterization. We plan to observe a grid of 4 x 4 points spaced at roughly 2' intervals. The observing time will vary as a function of off-axis ange. On-axis the expected countrate is 1 cps/module in the 40 – 79 keV band, so 2 hour integration is required to reach the requisite precision. The largest off-axis angle requires 36 hours of integration in order to characterize the PSF wings to 3% at high energy. This long integration will only be performed for two points and azimuthal symmetry will be assumed.

Effective Area Normalization

Note: this section will be updated when ground calibration results are available so final response matrices can be used for simulations.

For effective area normalization we require a steady source well characterized by other hard X-ray missions. The Crab is the only astronomical source that is sufficiently steady and bright at high energy for overall effective area determination. Although there is large dispersion in measured normalizations, we will adopt the RXTE measurement as the best absolute flux determination in the 2 – 60 keV band. We rely on the fact that we will have good relative effective area measurements for optics and focal plane over the entire NuSTAR energy band, so we can tie the normalization to RXTE and use the relative area knowledge to determine the higher energy spectrum.

We considered the tradeoff of using the pulsed flux vs. the integrated flux. Due to uncertainties in the pulse shape and change in spectral index as a function of pulse phase (Zhang and Cheng, 2001), we find that using the entire nebula plus pulsar emission poses fewer systematic uncertainties. The extended nature does complicate the analysis, particularly below 10 keV.

To get area on and off axis we plan a raster of points roughly 5 x 5 at 2' spacing [TBR]. If we consider statistical errors only 2 days of integration should be able to determine the normalization of the effective area to 10% over a 10 x 10 arcminute FOV, leaving 2 days of margin against the allocation. Note that this part of the plan will be updated after ground calibration is complete and accurate response files are available.

In addition to the Crab, NuSTAR will participate in coordinated cross-calibration campaigns with operating missions.

Appendix A
Instrument Dead Time and Maximum Data Rate

Table 1 summarizes the contributions to the instrument dead time fraction.

	CBE	Requirement
Shield veto fraction, s	0.014 (for 1.3 kHz veto rate, 27^o orbit)	<0.02
Charge pump reset (charge pump mode only), c	0.01	0.01
Event processing, e	$2e^{-3}$ sec/event	$5e^{-3}$ sec/event

The instrument dead time consists of resulting from the electronics not accepting events due to shield veto signals, preamplifier reset, and the time required for the MISC to process events. The dead time fraction at a particular count rate can be expressed as

$$DTF = [s(1-c)(1-eR) + c(1-s)(1-eR) + eR(1-s)(1-c)]$$

where s is the shield veto fraction, c is the charge pump reset fraction, e is the per event processing time, and R is the count rate in Hz in an individual telescope. Table 2 shows the dead time fraction CBE and requirements for a few reference countrates. The measured count rate is the predicted count rate multiplied by (1 – DTF).

R	DTF (CBE)(%)	DTF(reqmt)(%)
7	3.7	6.25
10	4.3	7.7
50	12	27
100	21.4	50
200	40.5	97
400	78.6	100

In addition to the dead time, the fixed bandwidth of the instrument to spacecraft data interface and the average data downlink rate impose additional constraints on the data rate. Figure X shows the typical X-ray event data size, and expected metrology system and housekeeping data rates.

It should be noted that fluxes can be measured even for sources with countrates high enough to result in 100% dead time. The electronics is configured such that the time interval from the end of event processing to the next event trigger is accurately measured. This will be done to an accuracy of 1 microsecond or better. So, if the focal plane is illuminated with 10,000 cps the flux can still be measured to 1%, even though only 400/s will be processed.

On the ground during observatory integration and test, the 460.8 kbps interface with the S/C will limit the data rate to about 450 counts/s/module. This will be achievable only if the dead time fraction is consistent with the CBE value, otherwise the maximum count rate will be reached at 200 counts/s/module (when the DTF approaches 100%).

On-orbit, the limiting factor for sustained high data rates is the S/C average telemetry downlink. At data rates higher than this, data will be discarded [by the instrument or S/C]. Current estimates are that early in the first month of the mission 9 Gbits/day of data from the instrument can be sent to the ground for an Equatorial orbit, and about 4 Gbits/day for the 27 degree orbit. Assuming an average observing efficiency of 50% due to Earth occultation and SAA passages data will have to be discarded for sources exceeding approximately 200 events/s/module.

APPENDIX B
Optics Calibration Procedure

1. Introduction

This document describes the calibration and functional testing planned for the flight optics modules constructed for the NuSTAR program. Functional testing is performed on the first flight module, FM0, before and after an environmental test program to validate the throughput and imaging characteristics of the optic under test. Calibration is performed on all three flight optics before delivery to JPL for integration. The test flow for the flight optics is shown in Table 1 below.

1.0 Test units

There are three optics flight units, designated as FM0, FM1 and FM2. FM0, which is completed first, will be available for calibration in early August 2010. As FM0 will be calibrated first, it provides a particularly useful test platform to validate procedures, integration times, assumptions about systematics and the validity of modeling. It is anticipated that FM0 testing will serve to close out any remaining TBC's/TBR's in this document, well in advance of the calibration of FM1 and FM2.

Test Article	Description	Date available	Measurements	Notes
FM0	133 layer multilayer coated optics module	August 2, 2010	Full calibration sequence; used to validate assumptions in this plan and to choose the minimum	Pt/SiC multilayers will provide poor response above 50 keV. Glass is selectively etched and has higher roughness

			sequence for FM1 and FM2	than the flight units. Will become flight spare if FM2 is completed on time in early January 2011
FM1	133 layer multilayer coated optics module	Jan 7, 2011	Full calibration	Pt/C multilayers on layers 1-93. W/Si on higher layers
FM2	133 layer multilayer coated optics module	Jan 21, 2010	Full calibration	Pt/C multilayers on layers 1-93. W/Si on higher layers

2. Calibration Overview

2.1 Basic assumptions

Time pressure is unavoidable for the optics calibration as both FM1 and FM2 modules are likely to on the mission's critical path. As extra time, above and beyond the allocated 10 days, is unlikely to be available as contingency, the plan has been designed with internal contingency on a nominal set of measurements; an irreducible minimum is also defined. An efficient set of measurements allows the choice between early delivery, and additions to the nominal plan which would result in more complete sampling of the optic as compared to the baseline set of measurements defined in this document.

The Nevis calibration facility is unique in that the resources available to build the facility were significantly limited compared to those that might be expected for such a facility. This has several implications for x-ray calibrations being performed there that drive the details of the calibration plan. The dominant concern results from the use of PVC pipe and roughing pumps to provide the vacuum for the beam, particularly for the 160m long main beam path (between source and optic). The pressure in this long pipe, which is nominally expected to be < 0.3 torr, varies as a function of distance along the beam line, with the number of pumps available at any one time, and with temperature and humidity conditions in the tunnel, leading to temporal and spatial variation of the attenuation, significantly affecting beam properties at energies below 10 keV. There is also a significant reliance on legacy hardware throughout the facility, with reuse of extant motion control components and other hardware throughout.

Because of the constraints described above, the calibration plan is designed with a reliance on simplicity in the design of measurements. The measurements are grouped into 5 types, and the overall approach is designed to use the most stable, and consistent, portion of the beam to minimize the effects for temporal variations in temperature and pressure. It should be noted that measurements at energies below 12 keV are particularly challenging. There are a number of lines in the source spectrum that require excellent spectral resolution of the detector for successful deconvolution. In addition, detector redistribution (off-diagonal response function) becomes significant for a high Z detector. For these reasons, and because of the long beam distance and relatively poor vacuum, the lower energy measurements are performed in a separate step, with a

separate detector (Si(Li) as opposed to Ge) and are focused on probing geometrical and contamination effects.

A number of changes in the beam geometry, including the use of He bags to bridge airgaps, and an extension of the vacuum pipe in the detector room, significantly decrease the attenuation at 6 keV from its baseline configuration. Even with those changes, however, the measurements are challenging. The current expected transmission of the beamline is shown in Figure 1 below.

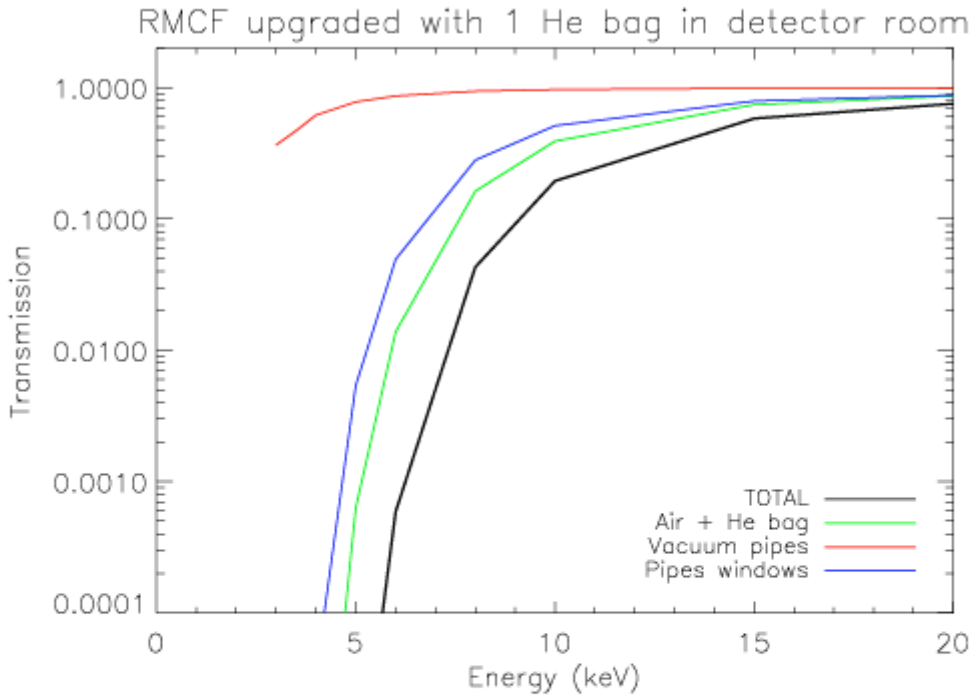

Figure 1: The current expected throughput of the Nevis beamline, from source to detector, with upgrades in vacuum tubes, He bags. Transmission in the vacuum tubes is based upon the currently achieved vacuums. Some improvement is possible with the addition of more pumps but this is a subdominant term.

We supplement the increased transmission of the beamline by adding a Si beam monitor to the Nevis beamline. This detector, a 25mm^2 0.5mm thick diode with a 1 mil Be window, provides good response from 5-20 keV and will be located at the focal plane. Additional correction of the low energy throughput will be made by interpolating environmental data (e.g. temperature, pressure and relative humidity) from the optics and detector rooms, as well as the pressure the in 10m pipe connecting the optics and detector cleanrooms.

We account for variation in the intensity of the beam as a function of time by requiring the frequent use of direct beam observations with the intention of producing standalone, normalizable data sets which are independent, to the degree possible, of conditions in the facility at the time of measurement. As experience is gained during the FM0 calibration; the possibility of easing the direct beam requirement is available and, based on that data, the exact sequence of the calibration for FM1 and FM2 could be adjusted. This would take place during a formal review of the FM0 calibration results; to be held in October of 2010, where the final calibration sequence for FM1 and FM2 will be proposed.

2.2 Optics Requirements

The optics Level 4 requirements are broken down here into two broad categories. The first, performance requirements, will be partially validated by measurement during the calibration (some will only be validated on-orbit). The second category, calibration requirements, is specific to how the on-ground calibration will be performed.

2.3 Performance Requirements

The derived optics performance requirements are:

Each optics module shall have an on-axis effective area that is greater than the values listed below at the indicated energies.

Energy [keV]	6	10	15	20	30	40	50	55	60	70	78
Area [cm^2]	402	394	262	201	135	99	71	60	50	34	22

ID : L4-OPTICS-32

The optics shall have an effective area, for a point source 873 microradian (3 arcminutes) off axis, no less than that specified in the table below.

Energy [keV]	6	10	20	30	40	50	60	75
Area [cm^2]	325	318	152	96	66	45	30	11

ID : L4-OPTICS-61

The optics shall have an effective area, for a point source 1745 microradian (6 arcminutes) off axis, no less than that specified in the table below.

Energy [keV]	6	10	20	30	40	50	60	75
Area [cm^2]	225	212	88	53	35	22	13	5

ID : L4-OPTICS-62

Each optic shall have an effective area, for a point source on-axis, no less than that specified in the table below.

Energy [keV]	66	67	68	68.5	69	70	71
Area [cm^2]	42	42	40	40	40	34	33

ID : L4-OPTICS-64

The point spread function of each optics module shall contain 50% of the collected photons from an on-axis point source to 208 microradian (43 arcseconds) diameter.
ID : L4-OPTICS-52

The point spread function of each optics module shall contain 70% of the photons from an on-axis point source to 363 microradians (75 arcseconds) diameter.
ID : L4-OPTICS-53

The point spread function of each optics module shall contain 80% of the photons from an on-axis point source to 485 microradians (100 arcseconds) diameter.
ID : L4-OPTICS-130

2.4 Ground Calibration Requirements

The derived calibration requirements for the optics at Level 4 are:

The optical axis of each optics module shall be coaligned to the optical boresight of that optics module to within +/- 50 microradians.
ID : L4-OPTICS-82

The percentage of X-ray throughput for each optics module shall be measured for at least 2 energies and for 3 angular positions (on-axis, 873 microradian off-axis, and 1745 microradians off-axis) at each of those energies to an accuracy of 5%.
ID : L4-OPTICS-84

Each optics modules shall have a focal length of 10150mm +/- 10 mm

Controller : Instrument Manager
ID : L4-OPTICS-148

The relative effective area of each optics module, for x-ray energies between 6 and 60 keV and over the central 8' by 8' of the field of view, shall be determined to at least 3% in each 2 keV bin.
ID : L4-OPTICS-150

The relative effective area of each optics module, for x-ray energies between 60 keV and over the central 8' by 8' of the field of view, shall be determined to at least 2% in each 1 keV bin.
ID : L4-OPTICS-151

3. Calibration Approach

3.1 Overview of Approach

The general approach is to place, within a limited portion of the beamline, an aperture which defines the beam. The optic is aligned to the beam, using X-rays, and the co-alignment of the mechanical and x-ray optical axes is validated. After alignment, the optic is positioned to the on-axis position and circular apertures, defining each of the 20 multilayer groups, are used to fully illuminate the optic. After these steps are complete, the detailed calibration of the optic begins and a small segment of the optic module under test (as defined by a separate static aperture plate affixed to the front of the optic) is translated to a well-defined portion of the beam and then aligned, in translation and rotation to set the correct radius and angle of incidence for the illuminating beam. A set of measurements (scanning in the yaw angle and at two beam energy/current settings) or, at times, a measurement at a single yaw angle and energy (as described in more detail in Section 4) are carried out at this position. The optic orientation is then adjusted to illuminate another section of the module. Measurements are repeated until a minimum subset of the area of the optics module is sampled.

Before and after each angular scan, and after each change in beam settings, the optic is translated out of the beam, and a measurement of the direct beam, through an appropriate aperture, with a precisely known geometry, is performed. These direct beam observations measure the flux and energy distribution of the beam at regular intervals and allow measurements to be normalized.

This sequence of measurements is followed by a separate, limited, set of measurements done at low energies. This separate measurement sequence uses a Si(Li) detector to provide the good low energy resolution required to resolve out the source spectrum and markedly reduces the effects of detector energy redistribution, since the fluorescence yield of Si is so much lower than Ge. The low energy measurements are the primary probes of the effects of geometry (i.e. spacer misalignment and epoxy fillets) as well as effects of contamination.

This baseline approach, hereafter ‘the baseline’, provides for direct measurement of a significant fraction of the optic with a beam that is directly measured before and after an observation, thereby providing a set of standalone measurements that are as nearly independent of beam and facility systematic as possible.

This baseline approach, however, does not provide the highest efficiency possible and, in particular, does not fully probe 100% of the optic at off-axis angles.. Accordingly, we will also carry out, on FM0, an alternate set of measurements, (hereafter 'the alternate') which is potentially more efficient and could potentially sample 100% of the optic area, and perform a detailed comparison of the results in preparation for the FM1 and FM2 flight model calibrations.

3.2 Types of measurement

There are 5 types of measurements that will be performed during the baseline calibration of the flight optics.

I. Direct beam: Measurements of the direct beam through a defining aperture, with the optic out of the beam. These measurements are typically 20 second integrations, performed at least once per hour during a calibration period, and are done before and after each angular scan and after any change in x-ray source parameters or other significant variations in facility conditions.

II. Baseline angular scan: These are the workhorse measurement and probe the mirror performance as a function of angle and energy. Measurements of a sector of the module (6 or 7 layers in radius, and an azimuthal arc consistent with the radius group under measurement) are made over a set of 9 angles ranging from near grazing incidence through an angle consistent with the edge of the flight CZTdetector plus 1 arcminute. The exact value of the angles measured in dependent on radius within the optic and will be established before FM0 calibration begins. Each angular scan is performed at two beam settings. The first has no filter installed and emphasizes the lower end of the energy spectrum. The second has a filter combination installed in the beam to bias the beam toward higher energy; the source current and voltage are also adjusted to produce more incident higher energy photons.

III. Baseline azimuthal check: Measurements of a sector of the mirror (6 or 7 layers in radius, and an azimuthal arc consistent with the radius group under measurement) at one angle, equal tothe nominal on-axis graze angle averaged over the group of layers being measured. These azimuthal checks sample a larger fraction of the mirror than the angular scans and, by duplicating at least one angle within the angular scan, allow the angular scans to be used for characterization of the azimuthal variation of the entire 6 layer group. These check observations are done with the 'low energy' beam setting and emphasize statistics at the lower energies (12-30 keV)

IV. Alignment observations: Measurements of the entire azimuthal (annular) extent of the mirror, with radial masking to select particular multilayer groups. These observations validate the alignment of the optical axis with the X-ray beam. The optic is rotated through roll, yaw and pitch and translated through X, Y to validate that the alignment is consistent with maximum throughput/symmetry. These alignment observation measurements provide a direct assessment of the integrated point spread function and will also be used as a check on interpolations and extrapolations from the baseline angular scans.

V. Point Spread Function Determination: Measurements of the diameter of the encircled energy contours, on-axis and at 3 off-axis positions. These are performed by finely sampled slit scans across the point spread function while setup for the angular alignment measurements. Depending on the availability of a 2-dimensional imaging detector (from RMD) imaging observations of the

point spread function will be performed as well (the two detectors are simply interchangeable in the Nevis calibration facility detector room).

3.3 Definition of coordinate systems

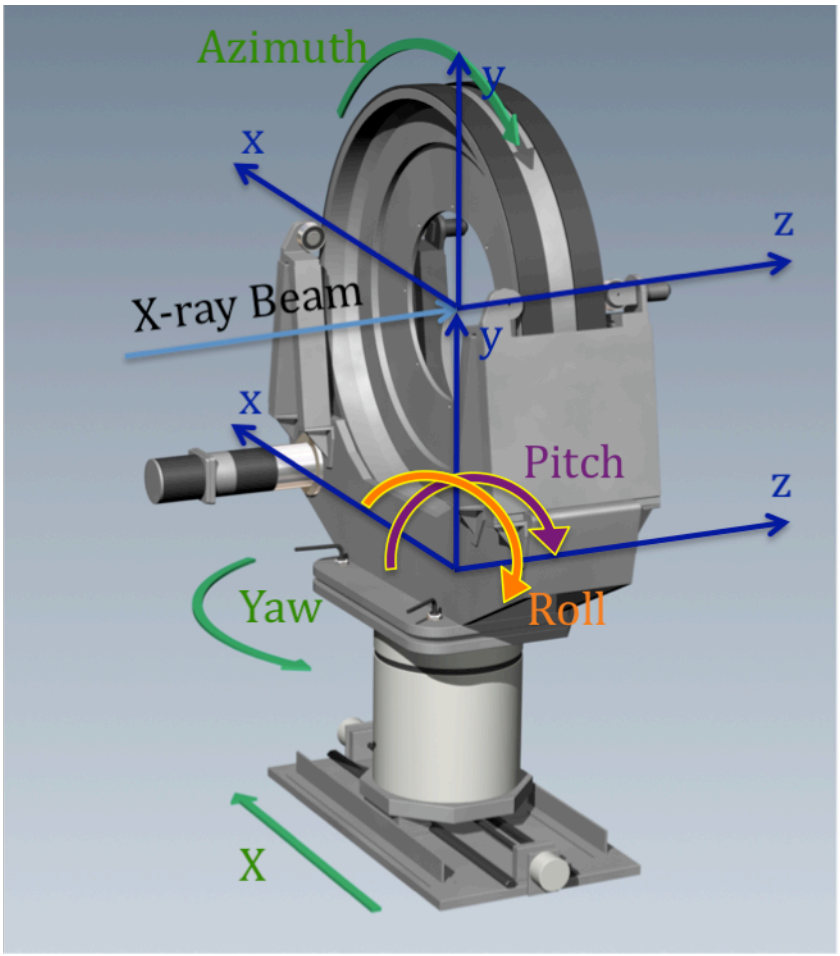

Figure 2: Definition of coordinate systems in reference to the optic holding fixture, the 'Danish Roll'

The center of coordinate system is at the midpoint of the optic when it is aligned with the x-ray beam line as determined by survey.

Using a right handed coordinate system as illustrated in the above figure:

- Z axis is aligned with the X-ray beam axis which is slanted at approximately ~1 degree with respect to the gravity normal and where positive is toward the detector,
- X axis is normal to the plane defined by the Z-axis and the gravity vector where positive to the east,
- Y axis is orthogonal to the X and Z axes where positive is in the 'up' direction at ~1deg relative to the gravity vector.

- Roll is a rotation about the Z axis (positive from the X to Y axis)
- Pitch is a rotation about the X axis (positive from the Y to Z axis)
- Yaw is a rotation about the Y axis (positive from the Z to X axis)

The center of coordinate system is at the midpoint of the optic when it is aligned with the x-ray beam line as determined by survey.

3.4 Definition of beam

To simplify the analysis of the measurement and to reduce systematics to the fullest extent possible we always utilize the same central portion of beam for the baseline calibration measurements (except for the special case of either alignment observations or point spread function measurements, which are not used to determine effective area).

If, after the calibration of FM0, with both baseline and alternate approaches, it is shown that beam or facility systematics are insignificant or controllable, a larger angular aperture could be used. In this case, the aperture stop would look more like an open wedge, to provide a uniform azimuthal sampling of the optic shells as a function of radius.

Figure 3: Schematic aperture stop, located directly upstream from the aperture plate, is used to limit the beam illuminated in both radius and azimuth in the baseline approach. The aperture

shown schematically here provides firm limits on the radial and azimuthal extent of the incoming beam. The aperture stop geometry and position can change for different radial groups to sample the same azimuthal span at all radii. The detailed design of this configurable stop is underway at this writing.

Aperture plates (as opposed to stops) are then used to define groups of ~6 radial layers. These aperture plates are pinned to the front of the optic and define, precisely, the shells being illuminated. The area of the aperture plate that is illuminated is defined by the static aperture stop, placed directly upstream of the aperture plate. Six aperture plates (each capable of illuminating 2 to 6 radially separated groups of layers) will be required. The azimuthal spans of the annular opening in the aperture plates are, in concert with the aperture stop, based on fixed angle ranges not fixed X,Y, in order to minimize exposure area uncertainty by using the spacer (1.6 or 1.2 mm) and spider (7 mm) azimuthal widths. In the baseline approach, no azimuthal span will exceed the height of the detector. This allows the direct beam illuminating the optic to be placed entirely on the detector. If beam uniformity is established, through a series of planned measurements, to be sufficient (over time and beam/facility conditions) to remove non-uniformity along the azimuthal arc as a significant error term, the azimuthal span may be increased, resulting in higher efficiency.

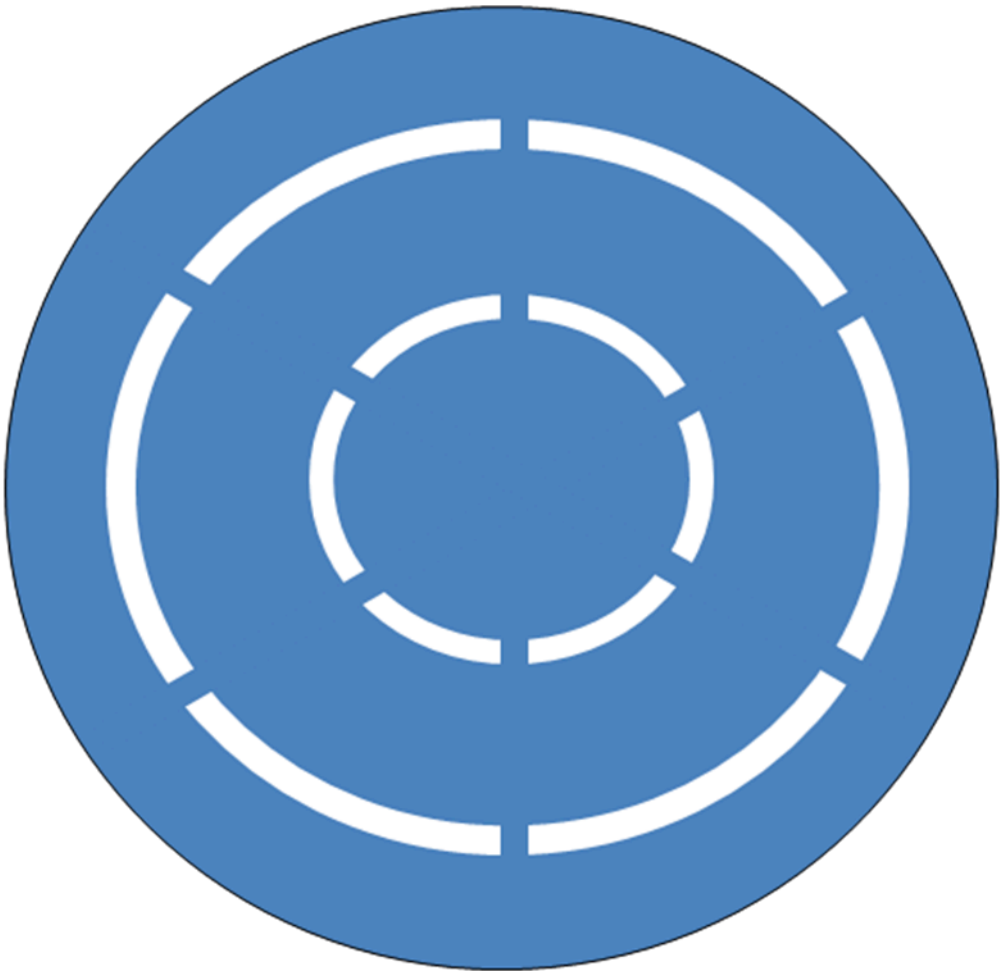

Figure 4: A notional aperture plate. The support members align with the gaps between sextants (i.e. the spider spokes). This platewould serve to illuminate two groups of layers, separated sufficiently in radius that only one group can be illuminated at a time through the aperture stop. More radial groups can be accommodated on a single plate if the radial groups not under investigation are separately occluded; see Figure 4 below:

3.5 Hardware requirements

Table 2: Summary of required hardware

Hardware Element	Location	Axes of motion	Extent of travel	Precision	Notes
X-ray filters	In beam, at source.	None	N/A	Coarse, filter position should repeat to +/- 1mm.	Filter material is TBD, to be procured commercially. Thickness of filters is 3mm. Remote operation of up to four 3mm thick filters is provided by JJ filter holder.
X-ray graded Z shaper/collimator	In beam, at source end, downstream from filter. Size of active element is 25mm x 25mm in X and Y and extent < 50mm in Z. Downstream is a 4mm thick collimator, of extent 50 x 50 mm in XY, with a circular opening of diameter 7mm	None	N/A, must be removable by hand.	Shall repeat to +/- 1mm when being reinserted by hand.	Several designs are possible for these graded Z structures. Collimator is used downstream of the filters and graded Z shapers to limit scattering from filter material. Can be aligned by hand one, and then should repeat to +/- 1mm.
Aperture stops	End of main	None	None.	Located to +/-	4 mm

	beam, prior to aperture plates and optic			0.5 mm with respect to the x-ray beam	Tantalum, Tungsten, Lead or equivalent where practical.
Aperture plate	Affixed to front of optic	None	None	Located to +/- 0.04mm in radius as referenced to optic center. Located to within +/- 1mm in azimuth.	
Optic	Origin of coordinate system	X (or Y) Yaw (or Pitch) Roll Pitch (or Yaw)	+300 to -10mm >+/- 18mrad 360 degrees >+/- 9mrad	+/- 0.025 mm +/- 5 μrad +/- 0.1 degree +/- 30 μrad	Repeatability Knowledge Repeatability Remote operation
Detector slit	Just before detector at Z ~ 10.1m	X Theta Width Z	+/- 30mm +/- 1 degree 0-10mm 10100mm	+/- 0.025 mm +/- 50 μrad +/- 0.01mm +/- 20 mm	
Detector	At focal distance	X	>200mm	+/- 0.025 mm	
Beam monitor	Just before optic	None	N/A	N/A	Fixed position

3.6 Metrology Requirements

The specifications as detailed in the table above are not particularly challenging, except for the measurements of the pitch and yaw angle of the optic. Once the exact implementation of the metrology has been designed, developed and tested, tolerances will be updated and the error budget recomputed.

3.7 Transmission of aperture plates

The nominal specification of the aperture stop/plates is for a minimum of 4 mm of tantalum, tungsten, or lead with 5 mm as a baseline thickness.

3.8 Windows on beam line

The window on the exit of the 160m beam line shall be sized to be consistent with illumination of the full optic during alignment. The window at the entrance to the detector room pipe shall be sized to accept the entire exit aperture of the optic. The exit window of the detector room pipe shall be no less than 100 x 350mm in size (with the 350mm axis aligned to the +X-axis of the facility).

3.9 Vacuum in beam line sectors

The vacuum shall be below 5 torr in the main beamline, and below 2 torr in the optic-detector beamline during any calibration.

3.10 Detector and data acquisition

The high energy detector is an Ortec Ge coax:

- GMX series Gamma-X HPGe: GMX25P4-70 (SN 20-TN9500)
- Preamplifier Model A257N (SN 08326455)
- HV filter Model 138EMI (SN 09043895)
- Beryllium Window = 0.5 mm
- Inactive Germanium = 0.3 um
- Detector Diameter = 58 mm
- Detector Length = 48 mm
- End Cap to Detector = 3 mm
- HV Bias = NEGATIVE 3500 V
- Resolution (FWHM) @ 1.33 MeV, Co60:
    - Manufacturer spec = 2.09 keV
    - Ortec measurement = 1.85 keV (with 6 us shaping)
- Resolution (FWHM) @ 22 keV, Cd109:
    - Manufacturer spec = 715 eV
    - Ortec measurement = 582 eV (with 6 us shaping)

Low energy detector:

SiLi parameters here, will be placed here once the detector, currently expected to be borrowed from NRL, is identified.

3.11 Source and Filter Parameters

For the measurements to be performed during the NuSTAR calibration, we will use at least three nominal beam parameters as defined in the table below.

Setting	Source Voltage	Source Current	Filter configuration	Notes
Medium	100 keV	10mA	A: TBD B: TBD C: open D: open	
High	100 keV	10mA	A: TBD B: TBD C: TBD D: open	
Low	40 keV	5mA	A: TBD B: TBD C:	

	TBD D: open
***All values are TBR, filter configuration is still in work**	

Source linearity and stability are still being determined. It is known that the source is repeatable, though non-linear, below a current of 1mA.

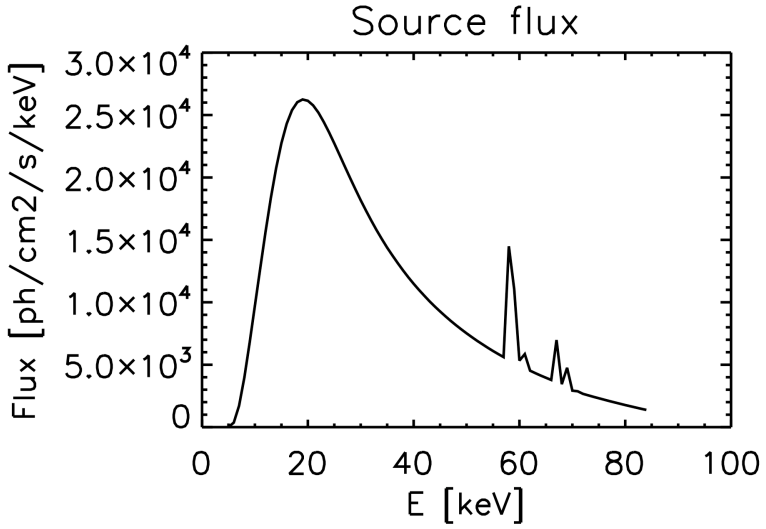

4.0 Calibration Implementation

4.1 Coordinate system

The first step in implementing the calibration plan is the establishment of a coordinate system. A survey of the beam line sets the line between the source position at the far end of the beam line and the center of the detector. All elements of the facility are then aligned to this fiducial line.

4.2 Installation and alignment of the optic; initial measurements

The optic is installed into a piece of GSE that provides a means to support, and adjust, the optic module on a translation/rotation fixture (hereafter, Danish Roll). The optic is mechanically attached and the pitch, yaw and roll axes of the optic are aligned such that a 360 degree roll about the optical axis does not produce more than 0.3mrad (TBC) of wobble in pitch and yaw (note that the pitch and yaw angles are finely adjusted for each measurement, the wobble requirement simply eases that fine adjustment step). The optic module is aligned to be within 0.3mrad (TBC) of the beam line axis and x-ray measurements begin.

4.2.1 Alignment measurements

All alignment observations are performed with annular aperture plates that allow the full illumination of each multilayer group in the optic. The first step in the process is a scan in pitch,

roll and yaw to confirm that the throughput of the optic is maximized when the x-ray beamline is aligned with the mechanical axis of the optic as set by the assembly process and validate requirement L4-OPT-82.

After the optic is verified to be 'on-axis', a series of measurement are performed through annular aperture plate which select out radial (multilayer) groups. As each multilayer group is sampled with a full annular illumination, the throughput of each group is measured directly.

4.2.2 Point Spread Function measurements

In conjunction with the alignment observations, point spread function measurements are performed. These measurements consists of a scan by a 0.2mm slit across the point spread function in the X direction for each aperture plate (multilayer group). In addition, a full flood illumination observation (with all aperture plates removed) shall be performed. If the RMD 2-dimensional detector is available during this period; PSF measurements shall also be obtained with that detector. The on-axis slit scans (or 2D integrations) will be repeated at 1, 3 and 5 arcminutes (TBC) off-axis to allow measurements of the point spread function on-axis and at 3 off axis positions.

Note that the source flux is quite high and both the alignment and point spread function measurements are detector count rate limited, i.e. the integrations are quite short. The time required to carry out these observations is driven by the rapidity of alignment and aperture plate installation but is expected to take, in total, no more than a few hours.

4.3 Response Measurement

With the optic installed and aligned, the next step is the definition of an illumination aperture. This is defined by combination of the aperture stop, and an aperture plate, both of which are changed as needed to define the specific layers being illuminated. The aperture plates are mechanically located with respect to the inner mandrel (mechanical axis) of the optics module and visually inspected to ensure that they are presenting the correct layers to the incoming beam.

With an aperture plate and stop in place, the sets of layers illuminated by that plate are measured. This measurement sequence is the primary calibration activity and is described in the following series of steps.

1) The first step in any measurement is the acquisition of a direct beam measurement. This measurement requires the use of an aperture, on the Danish Roll, that can be illuminated through the aperture stop while the optic is moved out of the beam and the detector is translated to the appropriate location.

2) An angular scan of a segment of the optic accurately measures the response of the multilayer coated optical surface as a function of both energy and angle. The optic is first rotated in roll to the desired orientation to illuminate a particular annular region (generally these will be aligned with the spacers that support the glass). The detector is translated to the appropriate position to intercept the focused beam and the detector slits are adjusted in width and angle as per the calculated settings for the measurement being performed. A

scan of the optic, in X, with the optic yaw set to on-axis, is performed to validate the placement of the aperture in X. With slit width set to the 'narrow' setting (defined as the width encompassing 70% of the point spread function) , nine 100 second integrations are performed at the 9 yaw positions specified in the calibration procedure for the particular aperture plate and radius in use (see Table XX for sample values). At the completion of the 9 scans, the yaw is returned to nominal on-axis position, and a100 second integration is performed. The slits are adjusted to the 'wide' setting (the wide setting is defined as the width encompassing 95% of the point spread function) and the 100 second integration is repeated. The slits are returned to the 'narrow' position.

3) The direct beam observation is repeated.
4) The input source spectrum is the biased toward high energy by inserting a low energy cutoff filter in the beam and the beam current is adjusted to produce optimal flux for this higher energy spectrum (all measurements are detector count rate limited). A direct beam observation is performed and steps 2 and 3 above are repeated.
5) The optic is then rotated, in roll, to a specified position (also aligned with respect to the glass support spacers) perform an angular check observation. Between 1 and 3 angular check observations are performed between angular scans, depending on radius. The angular check observation follows the setup process for an angular scan, however, only two integrations are performed, at the nominal on-axis yaw angle (TBC), one with slits at 'narrow' and one with slits at 'wide'. Only the 'low energy' beam setting is used during an angular check in order to constrain overall integration time. At the completion of the 1 to 3 angular check observations, the direct beam observation is repeated and, if the appropriate number of angular scans for that layer group are not yet completed, the next angular scan is performed.
6) When the 3 sets of angular scans/checks are completed, i.e. the optic has been sampled uniformly in azimuth, the optic is translated to the next radius (for that aperture plate) and the sequence of steps in 1) through 5) above is repeated.
7) When the layer groups in one aperture plate are completed, the aperture plate is removed and replaced with the next one in the sequence and the effort continued until all observations specified in the master measurement plan are completed.

NB: An alternate ordering of observations would be to keep the optic fixed in roll, and perform measurements of all the radial groups at a particular roll setting. The advantages and disadvantages of this approach vary with the exact implementation of metrology and apertures and unknowns in the systematics of the optic response. Both approaches will be enabled by the implementation of the motion control and aperture configuration and the final approach for calibration of FM1 and FM2 will be determined after FM0 data is available.

The table below summarizes the baseline calibration plan. The total time required, including setup and integration, totals less than 450 ksec for the baseline dual energy scan plus the low energy observations. This provides a factor of two contingency in the calibration period, assuming 1e6 seconds are available for calibration.

Layer Group	Nominal # of Angular Scans	Nominal # of Angular Checks	Time (seconds)	Mean radius (mm)	% of optic sampled
A	3	3	16020	56.1	78.27%
B	3	3	16020	59.6	73.66%
C	3	3	16020	63.6	69.03%
D	3	3	16020	67.8	64.78%
E	3	3	16020	72.2	60.86%
F	3	3	16020	76.7	57.24%
G	3	3	16020	81.5	53.89%
H	3	3	16020	86.5	50.79%
I	3	6	18420	91.7	71.85%
J	3	6	18420	97.1	67.82%
K	3	6	18420	102.8	64.07%
L	3	6	18420	108.8	60.56%
M	3	6	18420	115.0	57.29%
N	3	6	18420	121.5	54.22%
O	3	6	18420	128.3	51.35%
P	3	9	20820	135.4	64.87%
Q	3	9	20820	142.9	61.50%
R	3	9	20820	150.6	58.33%
S	3	9	20820	158.7	55.35%
T	3	9	20820	167.2	52.54%

Table XX: The nominal calibration sequence, totaling 360ksec. Assumptions are detailed in Table YY below.

Aperture extent (varies by radius)	Varies, direct beam never larger than 50mm in spatial extent
Direct Beam Integration time (seconds)	20
Direct beam setup time (seconds)	300

Angular Scan Integration time (seconds)	900
Angular scan setup time (seconds)	900
Angular check Integration time (seconds)	200
Angular check setup (seconds)	600
Aperture plate change time (seconds)	900

The baseline calibration plan provides for a factor of 2.0 in contingency time. If, due to schedule pressure or beamline availability, less time is available for calibration, the minimum subset of integrations would consist of 3 angular scans per layer group, plus enough angular checks to sample at least 40% of the optic area. If, due to schedule relief, or good beamline uptime, more time is available for calibration, the number of angular checks would be increased to achieve an optic sampling fraction of > 100% (i.e. provide full coverage, and as much overlap between angular checks as possible).

4.4 Low Energy Calibration

The baseline calibration sequence is followed by a sequence that emphasizes angular scans at low (< 12 keV) beam energy. Because of the low energy lines in the source spectrum, the more significant effects of detector redistribution, and the relatively coarse vacuum in the long beamline, these measurements will have higher errors in the determination of effective area, but have significant utility in probing the effects of specific geometry and of contamination on the optical surfaces. The baseline high energy detector (Ge coax) is replaced by a SiLi detector for measurements below 12 keV.

The low energy calibration sequence consists of a minimum of one angular scan per radial group. The angular scan consists of the sequence described earlier, with the addition of a pitch scan, performed over 7 steps in pitch, with the optic set at nominal yaw position. Although low energy performance of the beam is untested as this plan is being written, it is anticipated that this sequence can be completed in less than 90 ksec. Further refinement will be done once the details of the SiLi detector to be used are available.

The beam is monitored continuously at the entrance to the optic aperture by a Si diode described earlier.

4.5 Alternate Calibration Description

During calibration of FM0, the baseline calibration plan will be followed by an alternate calibration plan that has the primary difference that the azimuthal extent of

the beam is larger than the detector diameter to provide more areal coverage of the optic under test. In general the azimuthal extent will set for an entire sextant, i.e. it will be aligned with the spokes of the support spider. In this approach characterization of the direct beam, i.e. normalization, is inferred from a combination of measured beam stability and other characteristics.

The alternate plan has advantages in efficiency of area coverage, but the team believes that, at this writing, it could be more susceptible to unknown variations in beam or facility systematics as direct beam properties are inferred rather than directly measured. FM0, which will be calibrated using both methods, will provide the data to evaluate the final choice for the calibration of FM1 and FM2.

5.0 Error Budget

5.1 Error Budget Estimates

Chuck to fill in.

	Detector & X-ray Source Setting	Si	Si	Si+Ge_M	Ge_M+Ge_H	Ge_H
	Energy Range [keV]	6-8	8-12	12-25	25-55	55-78
1	Statistics	0.7%	0.7%	0.8%	0.7%	0.8%
2	X-ray Beam	2.1%	1.6%	0.8%	0.6%	0.8%
3	Detector & Electronics	0.7%	1.0%	0.8%	0.7%	1.0%
4	Optics	1.8%	1.8%	2.2%	2.1%	1.8%
	Total	**2.9%**	**2.7%**	**2.7%**	**2.7%**	**2.6%**
1	**Statistical**					
1.1	Measured Event Statistics	0.7%	0.7%	0.7%	0.7%	0.7%
1.2	Fitting Error: Detector Response Function Spectral Deconvolution	0.05%	0.05%	0.3%	0.2%	0.2%
1.3	Ambient Background Subtraction	0.05%	0.05%	0.05%	0.05%	0.2%
2	**X-ray Beam**					
2.1	Beamline Window Uniformity	1.0%	0.5%	0.2%	0.2%	0.2%
2.2	X-ray (Io) Source Spectral Stability	0.00%	0.00%	0.04%	0.18%	0.33%
2.3	X-ray (Io) Source Spatial Uniformity over Aperture	0.0%	0.0%	0.0%	0.0%	0.0%
2.4	Residual Error in X-ray throughput after Correction for Temp/Pressure/Humidity	1.5%	1.0%	0.5%	0.2%	0.2%
2.5	X-ray (Io) Beam Spectrum Model	0.2%	0.5%	0.2%	0.2%	0.5%
2.6	Finite Beam Size (including scatter throughout beamline)	1.0%	1.0%	0.5%	0.5%	0.5%
3	**Detector**					
3.1	Detector Electronics Energy Scale Integral Non-linearity	0.02%	0.41%	0.27%	0.18%	0.20%

3.2	Detector Energy Scale Integral Non-linearity	0.02%	0.41%	0.27%	0.18%	0.20%
3.3	Gain Drift between I and Io measurement	0.00%	0.00%	0.00%	0.00%	0.00%
3.4	Fitting Error Due to Finite Detector Energy Resolution	0.2%	0.5%	0.2%	0.2%	0.5%
3.5	Fitting Error due to Environmental Drift in Detector Energy Resolution	0.1%	0.2%	0.1%	0.1%	0.2%
3.6	Detector Response Function Systematic Error	0.1%	0.1%	0.2%	0.1%	0.1%
3.7	Detector Uniformity (including detector window)	0.2%	0.2%	0.2%	0.2%	0.5%
3.8	Deadtime Correction Uncertainty	0.3%	0.3%	0.3%	0.3%	0.3%
3.9	Pileup Correction Uncertainty	0.5%	0.5%	0.5%	0.5%	0.5%
4	**Optics**					
4.1	Optic Angular Alignment Uncertainty	1.0%	1.0%	1.0%	1.5%	1.5%
4.2	Optic Horizontal & Vertical Alignment -- combine with above	0.2%	0.2%	0.2%	0.2%	0.2%
4.3	Detector aperture Size Uncertainty	0.2%	0.2%	0.2%	0.2%	0.2%
4.4	Measurement Sampling/Addition	1.5%	1.5%	2.0%	1.5%	1.0%
4.5	Finite Distance Response Model	0.3%	0.3%	0.5%	1.0%	1.0%

1.1: total event statistics before detector response correction and background subtraction
1.2: statistical error in correcting (or alternatively fitting) the off-diagonal detector response; assumes known form for response function (see section 3)
1.3: measured ambient background ~0.1 cnts/sec/keV in calibration facility
2.1: Uncertainty in uniformity of beam windows under constant environmental conditions (includes thickness variation and bowing under vacuum)
2.2: Source spectral variation for a nominal 3C temperature change (Voltage Temp drift = 80 ppm/C, Current Temp drift = 50 ppm/C)
2.3: Uniformity of beam over aperture (or systematics in any necessary correction), under constant environmental conditions -- the X-ray source itself is expected to be perfectly uniform over the full optic aperture
2.4: Residual error in X-ray throughput after correcting for T,P,humidity
2.5: Contribution of W peak complexes in the 8-11 and 55-70 keV range to uncertainty in the (otherwise) smooth source spectrum model
2.6: Spot size = 3x5 mm, also includes scatter in air/windows which is simulated to be small -- only

3.1: DE = 0.05 keV (dA/dE*DE < 1.0%) -- Maximum deviation = integral non-linearity in energy calibration in the energy bands -- Canberra 2020 spec <+-0.05% for 2 us shaping
3.2: DE = 0.05 keV (dA/dE*DE < 1.0%) -- Maximum deviation = integral non-linearity in energy calibration in the energy bands -- get from Brian
3.3: I and Io measurements performed close together in time
3.4: ΔE ~ 1 keV for Ge & ~0.2 keV for Si (for I/Io dec volution)
3.5: dΔE = 5% peak width uncertainty (for I/Io decovolution)
3.6: Compton + K escape (for I/Io decovolution)
3.7: Relative Q.E. and attenuation uniformity of direct vs focused spot size
3.8: Deadtime measured directly from electronics si nal and pulser scheme
3.9: Residual pileup error in pile up rejection channel of TC244 spec amp
4.1: Assume ~4" misalignment
4.2: Changes position on detector
4.3: Sample more/less of PSF
4.4: Systematics in aperture size/alignment on optic & incomplete optic sampling
4.5: Correct for beam divergence (estimated from raytrace simulation)

APPENDIX C
NuSTAR Threshold Calibration

1. Introduction

This document describes the determination of the low-energy thresholds for each pixel. The ASIC that is used for NuSTAR uses a single parameter to set the threshold for all of its pixels (hereafter the "threshold set point"). Because of the variation in the pixel read out electronics, the value of the threshold will be different for each pixel.

The measurements presented below are designed to determine the threshold for each pixel for a given threshold set point. We simultaneously measure the electronic noise in each pixel and attempt to predict the achievable threshold for all pixels.

We report these results in the measured units (mV) as well as use the appropriate conversion between mV and photon energy to give the results in keV. The determination of pixel gain will be addressed elsewhere.

2. Overview

Each pixel is probed with a high precision DAC at a fixed set of voltages designed to sweep the input signal through the threshold for each pixel. The nominal range of voltages swept is 10.2 mV down to 1.8 mV in steps of 0.4 mV. At each location 200 pulses are triggered from the DAC and the number of triggers is recorded. For a trigger to occur, the DAC pulse must be above threshold. If the pulse were a delta function, then the transition between "above" and "below" the trigger threshold would be a step function. However, the DAC pulse in broadened by the Gaussian noise in the ASIC electronics.

The figure below shows experimental case in which we move a Gaussian distribution down in energy and compute the number of counts above threshold (upper panel) and the equivalent mathematical model in which we compute the cumulative sum of a Gaussian distribution as a function of increasing threshold. The latter is represented by the cumulative distribution function $F(x;\mu,\sigma^2)$ for a generic Gaussian-distributed function with mean μ and standard deviation σ:

$$F(x;\,\mu,\sigma^2) = \Phi\Big(\frac{x-\mu}{\sigma}\Big) = \frac{1}{2}\Big[\,1 + \operatorname{erf}\Big(\frac{x-\mu}{\sigma\sqrt{2}}\Big)\,\Big], \quad x \in \mathbb{R}.$$

We can then fit the fraction of counts above threshold with $F(x;\mu,\sigma^2)$ to determine the threshold and electronic noise for each pixel (bottom panel). This analysis is then repeated for each pixel to produce a threshold and electronic noise for each pixel.

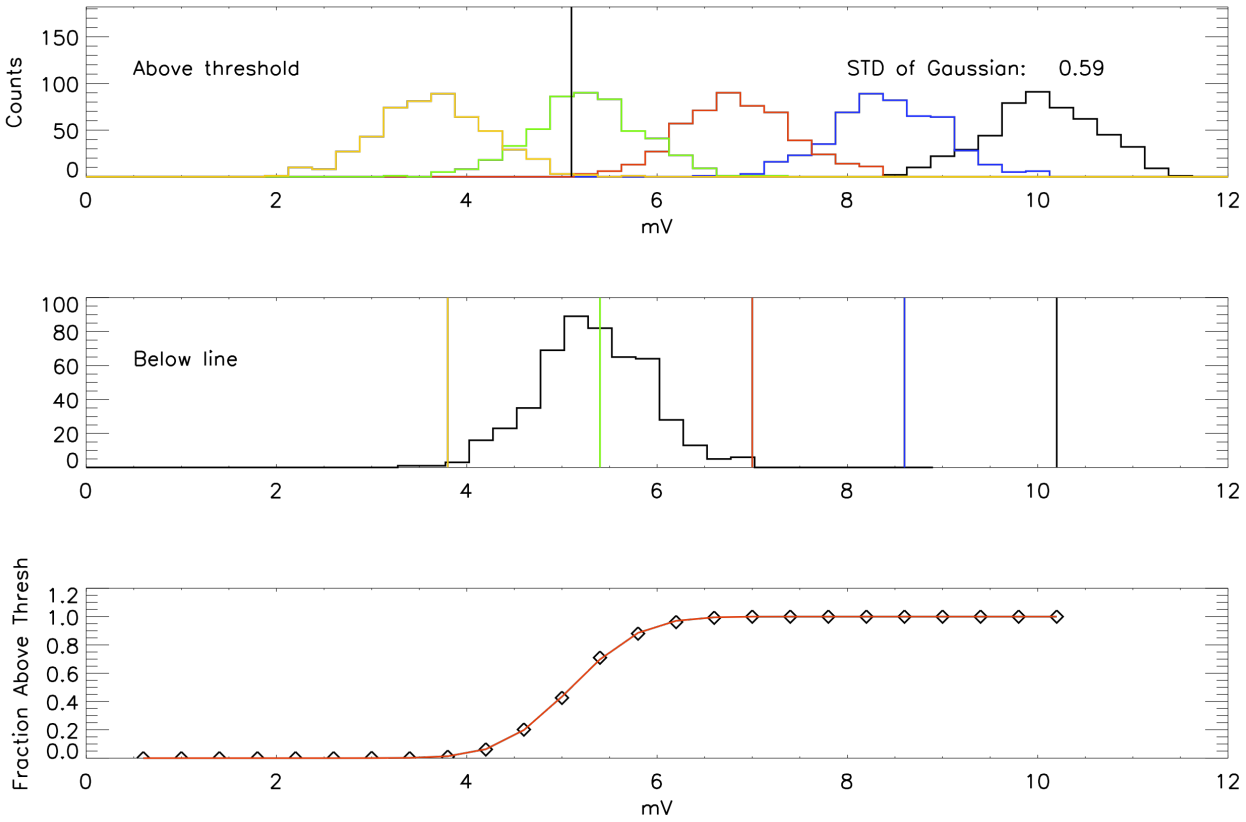

Figure 9: Simulation of the threshold data. Top Panel: Gaussian Distributions with changing mean voltage settings. The fraction above threshold is computed by integrated above the vertical black line. Middle panel: Stationary Gaussian function and changing threshold levels. The color codings correspond to the top panel, but here the data are integrated from -∞ to the threshold level to determine the cumulative distribution function. Bottom panel: Fraction of counts above threshold (diamonds) and the fit cumulative distribution function for a generic normally distributed random variable (red).

We performed a Monte Carlo simulation of this method with randomized threshold and noise settings. The RMS deviation of the computed threshold from the known threshold is 3 μV, while the RMS deviation of the computed electronic noise from the known noise is less than 0.1 μV.

3. Measurements

The data are taken several times during the ASIC and hybrid screening processes. The data shown here were taken with the hybrid near its optimal temperature setting (nominally 5 degrees C) and with the HV bias set at its nominal level of 500 Volts. Performing the test at these settings allows us to use calibration data to convert the threshold and noise from mV, which we measure, to keV.

Figure 2 below shows some representative data. Such data are obtained for all pixels, and the threshold and electronic noise recorded (Figures 3 and 4).

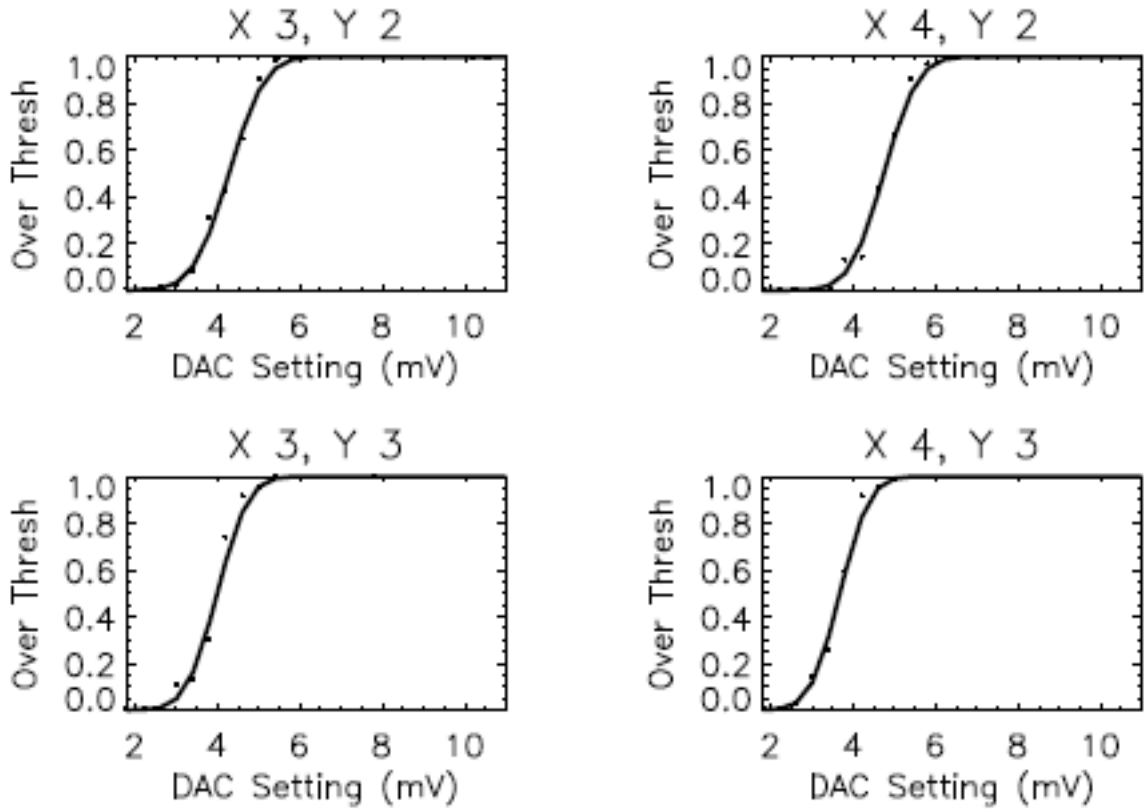

Figure 10: Fraction of counts over threshold as a function of threshold for several pixels on hybrid H21

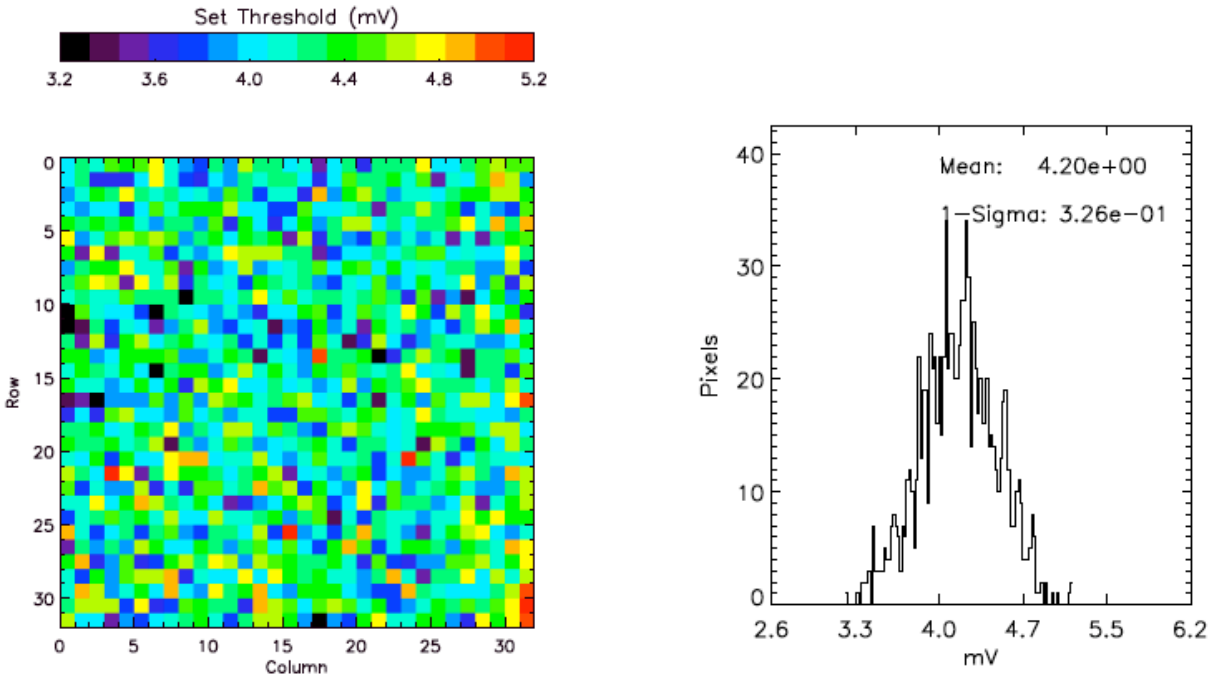

Figure 11: Left: Map of mean threshold values for each pixel, in mV. Right: Histogram of mean threshold values. Here the threshold set point is taken to be 4.2 mV.

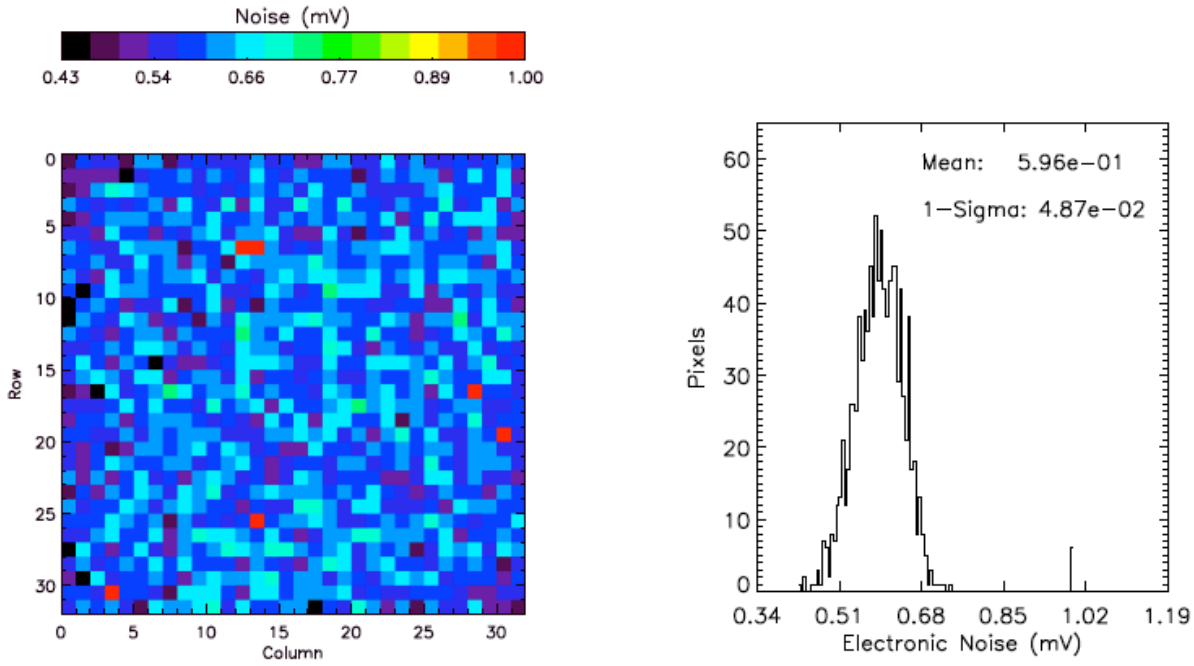

Figure 12: Left: Electronic noise for each pixel, in mV. Right: Histogram of measured electronic noise.

4. Conversion to keV

To convert the threshold measurement from mV from the DAC into a photon keV, we must apply a pixel-by-pixel conversion to account for the variations in readout electronics and in the intrinsic gain variations in the CZT. Figure 5 below shows the mV-to-keV gain for each pixel and a histogram of all of the gains. Figure 7 shows the current achieved threshold in keV for each pixel.

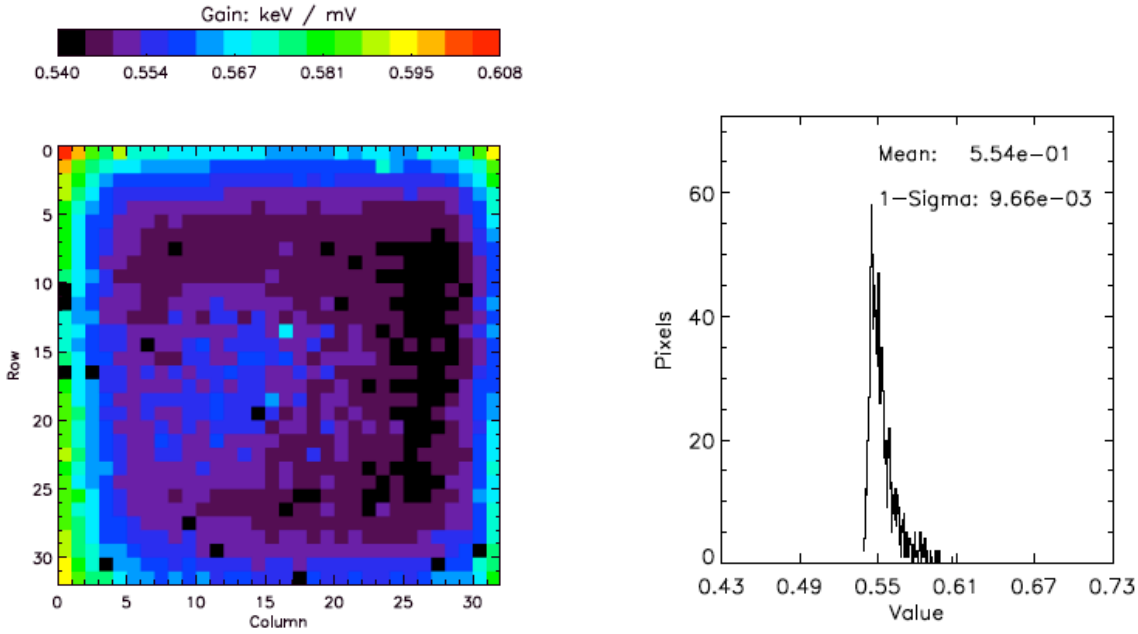

Figure 13: Left: Gain for each pixel. Right: Histogram of the gain of all pixels.

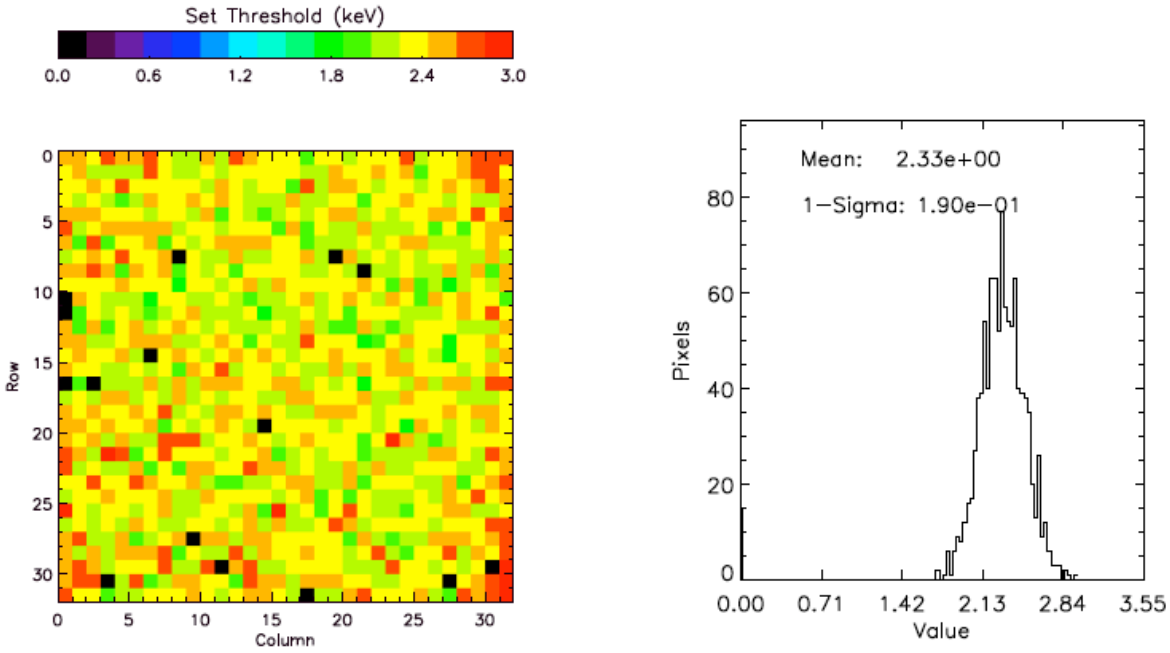

Figure 14: Threshold per pixel, in keV.